Nitric oxide-inducible Fe-S cluster biogenesis enables *Mycobacterium tuberculosis* to persist in mice

Kushi Anand[1], Ashutosh Tripathi[1], Kaustubh Shukla[2], Nitish Malhotra[3], Anilkumar Jamithireddy[4], Rajiv Kumar Jha[5], Susmit Narayan Chaudhury[3], Raju S Rajmani[1], Arati Ramesh[3], Valakunja Nagaraja[5], Balasubramanian Gopal[4], Ganesh Nagaraju[2] , Aswin Sai Narain Seshayee[3], and Amit Singh*[1, 5]

[1]Centre for Infectious Disease Research, Indian Institute of Science, Bangalore 560012, India. [2]Department of Biochemistry, Indian Institute of Science, Bangalore 560012, India. [3]National Centre for Biological Science, Bangalore 560065, India. [4]Molecular Biophysics Unit, Indian Institute of Science, Bangalore 560012, India. [5]Department of Microbiology and Cell Biology, Indian Institute of Science, Bangalore 560012, India.

***Correspondence**

Amit Singh, Ph.D
Associate Professor
Wellcome Trust-India Alliance Senior Fellow
Department of Microbiology and Cell Biology (MCBL)
Centre for Infectious Disease and Research (CIDR)
Indian Institute of Science (IISc)
Bangalore-12
Ph:+91 8022932604
asingh@iisc.ac.in

Abstract

Host-inducible nitric oxide (NO) suppresses *Mycobacterium tuberculosis* (*Mtb*) without eradicating it. Mechanisms underlying the persistence of residual bacteria in a hostile host environment are not known. Since NO damages Fe-S clusters of essential enzymes, the mechanism used to repair Fe-S clusters could help *Mtb* persist in host tissues. Here, we show that *Mtb* utilizes the *suf* operon (*Rv1460-Rv1466*) for Fe-S cluster biogenesis to persist under NO stress. Further, transcriptional repressor SufR (*Rv1460*) senses NO through its 4Fe-4S cluster to directly regulate Suf-meditated Fe-S cluster biogenesis. We discovered that NO inflicted irreversible damage upon Fe-S clusters to exhaust respiratory reserves and redox buffering capacity of *MtbΔsufR*. Importantly, *MtbΔsufR* failed to recover from a NO-induced non-growing state and displayed persistence defect inside immune-activated macrophages and murine lungs in a NO-dependent manner. Data suggest that SufR is a sensor of NO that supports persistence by reprogramming Fe-S cluster metabolism and bioenergetics of *Mtb*.

Introduction

About 90% of an estimated 2 billion people infected with *Mycobacterium tuberculosis* (*Mtb*) remain asymptomatic for tuberculosis (TB). This indicates that the host immune system effectively suppresses the pathogen's replication without eradicating the pathogen. The ability of the host to produce nitric oxide (NO) by an inducible nitric oxide synthase (iNOS) is known to modulate host immunity (1) and microbial physiology (2), thereby controlling diverse infections (3, 4) including TB (5). Upon infection with *Mtb*, lesional macrophages in humans and macaques express functional iNOS (6, 7), and exhaled breath of TB patient contains NO (8). Importantly, iNOS activity seems to control TB in humans (9, 10). Mechanistically, NO inhibits respiration and arrests growth of *Mtb* (2). The bacterial mechanisms responsible for sensing NO and mobilizing adaptation programs are poorly understood.

Previously published models suggest that *Mtb* exploits a three-component system, DosR/S/T, to induce transcriptional changes, growth arrest, and a switch from aerobic to anaerobic respiration to enhance survival under NO stress (11, 12). However, the NO-mediated activation of DosR regulon is transient(13) and other gases, such as carbon monoxide (CO) and oxygen (O_2-limitation), similarly activate the DosR pathway (14, 15). Therefore, the underlying regulatory mechanism that specifically coordinates changes in metabolism, growth, and respiration of *Mtb* in response to NO remains unknown.

81 NO is believed to affect bioenergetics by targeting heme, Fe-S clusters,
82 mycothiol, and protein thiols in *Mtb* (16). In this context, a recent study
83 demonstrated active degradation of several iron-sulfur cluster (Fe-S) proteins
84 coordinating respiration, central metabolism, and amino acid biosynthesis in
85 NO-treated *Mtb* (13). In addition, a seven-gene operon, the Suf system
86 (Rv1460-Rv1466) that is likely involved in Fe-S cluster biogenesis (17),
87 showed prolonged, elevated expression in response to NO (13). Other targets
88 of NO, such as haemoglobins, cytochrome C oxidase, and thiol proteins,
89 remained unaffected(13), supporting the significance of Fe-S cluster
90 homeostasis in remedying NO stress in *Mtb*. Moreover, NO modulates the
91 regulatory activity of two redox sensors, WhiB3 and WhiB1, by targeting their
92 Fe-S clusters (18-20). Since the reaction of NO with Fe-S clusters generates
93 a lethal dinitrosyl-iron dithiol complex (DNIC) (21), active degradation and
94 calibrated regeneration of Fe-S clusters via the *suf* operon represents a
95 potential adaptive defense against NO. Despite these reports, experimental
96 evidence showing a contribution of the *suf* operon in the bacterial response to
97 NO and coordination of Fe-S cluster biogenesis remains circumstantial (22,
98 23). Filling this knowledge gap is crucial to understanding the molecular
99 underpinning of persistence by this human pathogen.
100
101 In the present work we performed transcriptomics, Fe-S enzymatic
102 assays, bioenergetics flux analysis, and redox biosensor measurements to
103 identify the molecular underpinnings of *Mtb's* response to NO. We performed
104 a comprehensive analysis of an Fe-S cluster containing the transcription
105 factor SufR (Rv1460) and established that SufR-mediated regulation of Fe-S

106 cluster biogenesis organizes the bacterial response to NO. Finally, we
107 confirmed the requirement of SufR in promoting persistence of *Mtb* in
108 response to NO *in vivo*.

109

110 **Results**

111 **NO modulates the expression of Fe-S cluster pathways in *Mtb***
112
113 We performed transcriptomics of *Mtb* treated for 4 h with 0.5 mM of the
114 NO donor diethylenetriamine-nitric oxide (DETA-NO) by sequencing RNA
115 (RNA-seq). *Mtb* treated with 0.5 mM DETA-NO retained viability, but growth
116 was arrested (SI Appendix, Fig. S1). We identified significant changes in the
117 expression of 903 genes (fold change ≥ 2; FDR ≤ 0.05) (Data set 1A). Our
118 RNA-seq data recapitulated the central themes of the NO-responsive
119 transcriptome of *Mtb*, with induction of the DosR, IdeR, Zur, and CsoR
120 regulons, and with reduced expression of RNA and protein biosynthesis
121 pathways (SI Appendix, Fig. S2 and Data set 1A) (13). Since NO and its
122 congeners target lipids, DNA, and redox metabolism (24), genes involved in
123 redox homeostasis, lipid biosynthesis, and DNA repair were induced (SI
124 Appendix, Fig. S2 and Data set 1A).

125

126 Because iron is the principal transition metal that reacts with NO (25)
127 and since Fe-S cluster proteins are the most susceptible targets of NO (26),
128 we examined the expression of 76 genes encoding the Fe-S cluster proteome
129 of *Mtb* (Data set 1B). We discovered altered expression of 35 genes, 23 being
130 up-regulated and 12 down-regulated in response to NO (fold change ≥ 1.5;
131 FDR ≤ 0.05; Fig. 1 and Data set 1B). Genes encoding Fe-S enzymes involved

132 in central metabolism (*acn*, *prsA*, and *udgA*) and primary respiration (*nuo*
133 operon) were down-regulated, whereas genes mediating alternate respiration
134 (*narH*, *sirA, fdxA, hycP, and fdxC*) (27), alternate carbon catabolism (*korAB*,
135 *frdB*) (28), and redox metabolism (*rubA-B*, *cysH*, and *nadA-B*) (29-31) were
136 induced by NO (Fig. 1; Data set 1B). NO also induces *thiC*, which encodes a
137 Fe-S cluster-containing enzyme that generates thiamin and thiamin-
138 dependent branched chain keto-acid dehydrogenase complex (BCKADH)
139 (Fig. 1). Catabolism of branched chain amino acids (BCAAs) by BCKADH
140 generates acetyl-CoA and propionyl-CoA (32), which fuel the glyoxylate cycle,
141 methyl citrate cycle, and gluconeogenesis (33). Consistent with this, NO
142 induces the expression of genes coordinating BCAAs biogenesis,
143 glyoxylate/methyl-citrate cycles (isocitrate lyase [*icl1*]), and gluconeogenesis
144 (PEP-carboxykinase [*pckA*]) in *Mtb* (Fig. 1; Data set 1A).
145
146 The strong reactivity of NO toward the heme iron of primary
147 cytochrome oxidase is thought to arrest respiration (2). We found that NO
148 does not affect the expression of primary terminal oxidase (cytochrome bc1-
149 aa3 complex; *qcrABC*) in *Mtb* (Fig. 1). However, the expression of alternate
150 respiratory complexes (*e.g.,* NADH dehydrogenase type II [*ndh*] and
151 cytochrome BD oxidase [*cydABCD*]) (Fig.1) (34) was induced. Genes of Fe-S
152 cluster enzymes producing cofactors for respiratory quinones (isoprenoid;
153 *lytB2*, *gcpE*) (35) and nitrate reductase (molybdopterin; *moaA2*) (35) were up-
154 regulated by NO (Fig. 1). Expression of transcription factors containing NO-
155 sensitive Fe-S clusters (*e.g., whiB1, whiB2, and whiB3)* was induced (18, 20,
156 36) (Fig. 1). Up-regulation of the Fe-S cluster transcriptome indicates an

157 increased demand for Fe-S cluster biogenesis. In agreement, expression of
158 the *suf* operon (*sufRBDCSUT*; Rv1461-Rv1466) was stimulated 15 to 25-fold
159 by NO (Fig. 1). Also, NO induces the cysteine biosynthetic machinery that
160 supplies sulfur for Fe-S cluster biogenesis (Fig. 1). In contrast, genes
161 coordinating biosynthesis of Fe-binding heme (*hemZ*) and encoding Fe-
162 storage proteins (bacterioferretin; *bfrA-B*) were down-regulated (Fig. 1). These
163 observations, along with strong induction of the *ideR*-mediated iron starvation
164 response, suggest that *Mtb* faces Fe scarcity under NO stress and manages it
165 by prioritizing the assembly of [Fe-S] clusters.
166
167 **NO modulates activity of Fe-S cluster enzyme, bioenergetics, and redox**
168 **potential of *Mtb***
169 Altered expression of the Fe-S pathways involved in metabolism and
170 respiration by NO indicates that NO might modulate these processes in *Mtb*.
171 To investigate this idea, we evaluated the activity of a 4Fe-4S-containing
172 enzyme aconitase (Acn), which functions as a critical gatekeeper of the TCA
173 cycle, and shows sensitivity to NO due to a solvent-exposed Fe atom (37). A
174 gradual decrease in Acn activity over time was observed in *Mtb* exposed to
175 0.5 mM of DETA-NO, indicating Fe-S cluster damage. At 12 h post-exposure,
176 DETA-NO triggered a 40% reduction in Acn activity without decreasing its
177 abundance (Fig. 2a). Importantly, re-culturing DETA-NO-treated *Mtb* in a
178 DETA-NO-free medium significantly restored Acn activity, indicating efficient
179 mobilization of Fe-S cluster regeneration machinery (Fig. 2a).
180

181 Fe-S enzymes coordinate carbon catabolism and oxidative
182 phosphorylation (OXHPHOS) (38). Therefore, we exploited Seahorse XF Flux
183 technology to analyze the influence of NO on oxygen consumption rate (OCR)
184 and extracellular acidification rate (ECAR), which are measurable readouts of
185 OXPHOS and glycolysis, respectively (39). To quantify the basal and
186 maximum rates of OCR and ECAR, we cultured *Mtb* in 7H9-glucose in an XF
187 microchamber, then exposed it to DETA-NO, and finally to the uncoupler
188 carbonyl cyanide m-chlorophenyl hydrazine (CCCP) (Fig. 2b-c). Addition of
189 CCCP stimulates respiration to the maximal capacity manageable by *Mtb*.
190 The difference between basal and CCCP-induced OCR provides an estimate
191 of the spare respiratory capacity (SRC) available for sustaining stress-
192 mediated bioenergetics (*e.g.,* RNI and ROI) (40). Under normal growing
193 conditions, *Mtb* displays a basal OCR of 20±0.14 pmoles/min, which
194 increases to 85±11.7 pmoles/min in response to uncoupling stress by CCCP
195 (Fig. 2b). Similarly, basal ECAR increases from 4.5±0.48 mpH/min to 25±4.4
196 mpH/min in response to CCCP (Fig. 2c). These data indicate that *Mtb*
197 functions at submaximal OXPHOS (~ 25%) and glycolytic (~ 20%) capacities
198 under normal growing conditions. As seen with the uncoupler CCCP,
199 pretreatment with DETA-NO also increased basal OCR in a dose-dependent
200 manner (Fig. 2b). Also, DETA-NO pretreatment progressively reduces the
201 ability of *Mtb* to increase OCR or ECAR in response to CCCP (Fig. 2b and
202 2c). As a result, DETA-NO significantly decreased SRC in a dose-dependent
203 manner (Fig. 2d), indicating that *Mtb* mobilizes its reserved respiratory
204 capacity to sustain bioenergetics in response to NO. Our data indicate that

205 NO depolarizes the cytoplasmic membrane and activates respiratory reserves
206 of *Mtb*.
207
208 Lastly, we asked whether NO perturbs redox homeostasis in *Mtb*. We
209 used a genetic biosensor (Mrx1-roGFP2) to measure the redox potential of a
210 physiologically relevant antioxidant, mycothiol (MSH), as a proxy for the
211 cytoplasmic redox potential (E_{MSH}) of *Mtb* (41). Any change in redox
212 physiology can be easily quantified by ratiometric measurements of emission
213 at 510 nm after excitation at 405 and 488 nm (41). In response to an oxidant
214 or a reductant, the biosensor ratio showed a rapid increase or decrease,
215 respectively (41). *Mtb* expressing Mrx1-roGFP2 was treated with 0.25 mM,
216 0.5 mM, and 1 mM DETA-NO, and the biosensor ratio was measured. NO
217 exposure induces an insignificant increase in the Mrx1-roGFP2 ratio,
218 indicating that *Mtb* robustly maintains cytoplasmic E_{MSH} in response to NO
219 (Fig. 2e). Using a ROS-sensitive fluorescent dye CellROX, we confirmed that
220 NO induces a negligible increase in oxidative stress (Fig. 2f). Overall, the data
221 indicate that NO-induced growth arrest is linked to modulation of cumulative
222 respiratory and metabolic capacities of *Mtb*.
223

224 **SufR regulates the *suf* operon and the DosR regulon in response to NO**

225 Our gene expression and biochemical data indicate that Fe-S cluster
226 homeostasis is likely to be important for *Mtb's* response towards NO. To
227 examine this possibility, we investigated the role of *Mtb* SufR, which is a
228 putative regulator of the *suf* operon involved in Fe-S cluster biogenesis (23).
229 The *suf* operon, including *sufR*, showed a maximal and a long-lasting

230 induction in response to NO (13). Except for *sufR*, other genes of the *suf*
231 operon are essential (17). Therefore, we utilized previously reported
232 *MtbΔsufR* and *sufR*-complemented (*sufR-Comp*) strains (42) and performed
233 RNA-Seq in response to NO. As with wt *Mtb*, 0.5 mM DETA-NO arrested the
234 growth of *MtbΔsufR* and *sufR-Comp* without affecting viability (SI Appendix,
235 Fig. S3). Similar to wt *Mtb*, NO similarly affected the expression of the *ideR*,
236 *zurR*, and *csoR/ricR* regulons, carbon metabolism, protein biosynthesis, and
237 respiratory enzymes in *MtbΔsufR* (SI Appendix, Fig. S4, Data set 1C). A direct
238 comparison of *MtbΔsufR* with wt *Mtb* after DETA-NO treatment revealed
239 differential regulation of 67 genes (fold change ≥ 1.5; FDR ≤0.05) (Fig. 3 and
240 Data set 1D). Several genes of the DosR regulon showed hyper-induction
241 (≥1.5-fold; FDR ≤0.05) in *MtbΔsufR* as compared to wt *Mtb* or *sufR-Comp*
242 under NO stress (Fig. 3). More importantly, NO-specific induction of the *suf*
243 operon was absent in *MtbΔsufR* (Fig. 3). Because SufR is a putative
244 repressor of the *suf* operon (23), the diminished expression of the *suf* operon
245 in *MtbΔsufR* was unexpected. It is likely that by removing 345 bp internal to
246 the *sufR* ORF (+308 to +653 bp) for constructing *MtbΔsufR,* we might have
247 interrupted the formation of the NO-inducible transcript of the *suf* operon in
248 *MtbΔsufR* (SI Appendix, Fig. S5a). However, expression of the operon
249 remained at a low-level due to an additional transcription start site (TSS2)
250 upstream of Rv1461 (*sufB*) (SI Appendix, Fig. S5a). Consistent with this, the
251 aberrant transcript originated from the primary TSS (TSS1) and encompasses
252 the undeleted region of the *suf* operon (+1 to +307 bp) that remains induced
253 in NO treated *MtbΔsufR* (SI Appendix, Fig. S5a-b). As expected, the
254 expression of a native copy of *sufR* in *sufR-Comp* only restored the induction

255 of *sufR* in response to NO whereas rest of the operon remains uninduced
256 (Fig. 3).

257

258 While the *suf* operon involved in Fe-S cluster biogenesis was down-
259 regulated, the expression of pathways requiring Fe-S clusters remained
260 induced in NO-treated *MtbΔsufR* (Fig. 3). Thus, we anticipate that the
261 heightened demand for Fe-S clusters under NO stress is unlikely to be
262 satisfied in *MtbΔsufR*. Lastly, genes encoding surface antigens (*mpt70*,
263 *mpt83*, and *fbpc*), PE-PGRS family, and redox-sensitive transcription factors
264 (*oxyS* and *Rv3334*) (43, 44) were also down regulated in NO-treated
265 *MtbΔsufR* (Fig. 3 and Data set 1D). We also found that the expression of
266 nearly 50% of genes showing differential regulation in *MtbΔsufR* was restored
267 to approximately wt *Mtb* levels in the *sufR-Comp* strain under NO stress (Fig.
268 3 and Data set 1D). Since the *suf* operon remained repressed in *sufR-Comp*,
269 the partial complementation could be due to impaired activity of other
270 transcription factors (*e.g.,* WhiB1 and WhiB3) that require Fe-S clusters to
271 regulate gene expression in response to NO (18, 45). Altogether, the data
272 indicate that SufR adjusts the expression of the Suf Fe-S cluster assembly
273 system and the Dos regulon upon NO stress.

274

275 **SufR is required to maintain Fe-S cluster homeostasis, bioenergetic**
276 **reserves, and redox potential in response to NO**

277 Transcriptional data indicate altered Fe-S cluster homeostasis in
278 *MtbΔsufR*. We directly tested this idea by measuring the enzymatic activity of

279 Acn (a Fe-S enzyme) in *MtbΔsufR* under NO stress (Fig. 4). Compared to wt
280 *Mtb*, a similar decrease in Acn activity was observed in *MtbΔsufR* under NO
281 stress (Fig. 4a). However, and in contrast to wt *Mtb*, reactivation of Acn upon
282 removal of NO stress was absent in *MtbΔsufR* (Fig. 4a). Data suggest that
283 defective induction of the *suf* operon impairs regeneration of NO-damaged
284 Fe-S clusters in *MtbΔsufR*. As expected, *sufR-Comp* which lacks induction of
285 the *suf* operon in response to NO, did not reinstate Acn activity (SI Appendix,
286 Fig. S6).

287

288 Next, we measured OCR, ECAR, and SRC of *MtbΔsufR* in response to
289 NO as described earlier. Under normal growing conditions, *MtbΔsufR* utilizes
290 ~ 35% of its maximal respiratory capacity, which is significantly higher than
291 *Mtb* (~ 25%) (Fig. 4b). As a consequence, the SRC of *MtbΔsufR* was 2-fold
292 lower as compared to wt *Mtb* under standard culture conditions (Fig. 4c).
293 Moreover, while 1 mM of DETA-NO was required to significantly increase
294 basal OCR of wt *Mtb*, 0.25 mM was sufficient for *MtbΔsufR* (Fig. 4b). This
295 suggests that *MtbΔsufR* is more sensitive to membrane depolarization by NO.
296 Likewise, SRC was significantly diminished in *MtbΔsufR* as compared to wt
297 *Mtb* upon treatment with 0.25 mM of DETA-NO (Fig. 4c). Data demonstrate
298 that decreased SRC of *MtbΔsufR* increased its vulnerability towards
299 bioenergetic exhaustion under NO stress. However, unlike wt *Mtb*, *MtbΔsufR*
300 significantly increases basal ECAR and retains CCCP-induced ECAR in
301 response to 0.25 mM and 0.5 mM of DETA-NO (Fig. 4d). This suggests an
302 increased reliance of *MtbΔsufR* on glycolysis to handle the bioenergetic
303 needs under NO stress. Lastly, using the Mrx1-roGFP2 biosensor, we

304 measured E_{MSH} of *MtbΔsufR* in response to NO. We observed that NO
305 induces a slightly higher oxidative shift in E_{MSH} of *MtbΔsufR* than wt *Mtb* in a
306 dose-dependent manner (Fig. 4e). Consistent with this, staining with the dye
307 CellROX also indicated higher oxidative stress in NO-treated *MtbΔsufR* as
308 compared to wt *Mtb* (Fig. 4f). Altogether, our data indicate that SufR is
309 required to regenerate Fe-S clusters, maintain respiratory reserves, and buffer
310 redox imbalance to counteract NO stress.

311

312 **SufR mediates adaptation to NO stress *in vivo***

313 Next, we investigated the biological consequence of compromised Fe-
314 S homeostasis and bioenergetics by assessing the phenotype of *MtbΔsufR*
315 under NO stress. A single dose of various concentrations of DETA-NO (0.5
316 mM, 1.25 mM, and 2.5 mM) did not influence the survival of *MtbΔsufR* (Fig.
317 5a). Repeated exposure to low doses of NO is known to arrest the growth of
318 *Mtb* for an extended duration (46). Administration of 0.1 mM of DETA-NO
319 every 6 h for 36 h induces an extended period of growth arrest followed by
320 recovery of wt *Mtb* at day 7 post-treatment (Fig. 5b). In contrast, *MtbΔsufR*
321 resumed growth only at day 16 post-treatment with NO (Fig. 5b). The *sufR-*
322 *comp* strain showed a recovery defect similar to *MtbΔsufR*, indicating that the
323 NO-mediated induction of the entire *suf* operon rather than only *sufR* is
324 necessary for the timely resumption of growth. We confirmed this by reducing
325 the expression of another *suf* operon gene *sufT* involved in Fe-S cluster
326 maturation (47) using CRISPR interference (CRIPSRi-*sufT*). Reduced *sufT*
327 levels significantly delayed recovery of *Mtb* from NO-induced growth inhibition
328 (Fig. 5c).

329

330 Immunologically activated macrophages are known to induce nitrosative
331 stress in *Mtb* (48). In line with this, *MtbΔsufR* showed 10- and 40- fold
332 reduced survival in immune-activated Raw264.7 macrophages as compared
333 to wt *Mtb* at day 2 and 4 post-infection, respectively (Fig. 5d). These
334 observations prompted us to investigate the NO-dependent phenotype of
335 *MtbΔsufR in vivo*. WT *Mtb* and *MtbΔsufR* showed comparable growth in the
336 lungs of BALB/c mice during the acute phase of infection (0-2 weeks) (Fig.
337 5e). However, *MtbΔsufR* was cleared progressively from the lungs, with a
338 more than 1.5-log decline in bacterial burden by 8 weeks (Fig. 5e). The
339 persistence defect of *MtbΔsufR* was partially rescued in the case of animals
340 infected with *sufR-Comp* (Fig. 5e). Since *sufR-Comp* did not restore the
341 induction of the *suf* operon, the partial complementation is likely due to
342 restored expression of other *sufR*-specific genes (*e.g.,* DosR regulon). The
343 histopathological changes observed in the lungs of animals at 8 weeks post-
344 infection were proportionate to the bacterial burden (SI Appendix, Fig. S7a).
345 The magnitude of pulmonary damage was highest in case of wt *Mtb*
346 (2.75±0.5), intermediate in *sufR*-Comp (2.0 ±0.0), and lowest in *MtbΔsufR*
347 (0.25±0.50) (SI Appendix, Fig. S7b). Lastly, to clarify the role of NO in the
348 persistence defect of *MtbΔsufR*, we infected a highly susceptible mouse strain
349 lacking inducible nitric oxide (iNOS$^{-/-}$) (5). We found that the phenotypic defect
350 of *MtbΔsufR* was abolished in iNOS$^{-/-}$ mouse, indicating the requirement of
351 SufR for the persistence of *Mtb* in response to NO (Fig. 5f-g).

352

353

354 **Mechanism of SufR mediated regulation of Fe-S biogenesis**

355 Having confirmed the role of SufR in regulating Fe-S homeostasis,
356 bioenergetics, and *in vivo* persistence, we next sought to understand the
357 underlying biochemical and molecular mechanisms. Biochemical
358 characterization of SufR revealed the presence of a 4Fe-4S cluster. We
359 present data to demonstrate how the 4Fe-4S cluster in SufR serves as a
360 sensor for NO and H_2O_2 to modulate DNA binding and transcriptional
361 activity. These studies, which also allowed us to identify the DNA sequence
362 motif required for SufR binding, provide a basis for a mechanistic model for
363 SufR. The data and analysis leading to this model are described below.

364

365 **SufR contains a 4Fe-4S cluster**

366 We anaerobically purified histidine-tagged SufR from *E.coli* cultured in
367 growth conditions optimized for the maximum incorporation of Fe-S clusters *in*
368 *vivo* (49). As isolated, native SufR displayed a characteristic straw brown
369 color, with an absorption maximum indicative of a 4Fe-4S cluster at 413 nm
370 (molar absorption coefficient [ε] at 413 =16200 M^{-1} cm^{-1}) (Fig. 6a and SI
371 Appendix, Fig. S8) (18). Treatment of native SufR with a one-electron donor,
372 sodium dithionite (DTH), caused partial bleaching of brown color and loss of
373 absorbance at 413 nm, consistent with the presence of a redox-responsive
374 4Fe-4S cluster (18) (Fig. 6a). Gel-filtration performed under anaerobic
375 conditions suggested a molecular mass of ~ 54 kDa for native SufR, which is
376 consistent with a dimer. Clusterless SufR (apo-SufR) also eluted as a dimer,
377 indicating that the Fe-S cluster does not bridge SufR monomers (Fig. 6b).

378 Moreover, the identity of cysteine residues that coordinates the 4Fe-4S cluster
379 were experimentally validated. The alanine mutants of three putative cysteine
380 ligands (C175A, C179A and C192A) were seen to disrupt the 4Fe-4S cluster
381 as evident from the loss of absorbance at 413 nm (Fig 6c).

382

383 A previous study, using aerobically purified SufR and *in vitro*
384 reconstitution of Fe-S cluster, showed the presence of a 2Fe-2S cluster on
385 SufR (23). Since Fe-S clusters are susceptible to O_2 (50), our technique of
386 assembling Fe-S cluster *in vivo* followed by anaerobic purification is more
387 likely to provide native configuration of SufR Fe-S cluster. We further clarified
388 this by analyzing native SufR using circular dichroism (CD). The far-UV CD
389 spectrum shows two minima at 208 and 224 nm and indicates the presence of
390 70% α-helical content in the secondary structure (Fig. 6d). The near-UV CD
391 spectrum displayed two characteristic maxima at 330 and 420 nm and minima
392 near 550 nm as described earlier for [4Fe-4S] cluster (51) (Fig. 6e). As
393 expected, the near-UV CD spectrum of apo-SufR did not show the absorption
394 characteristics of a [4Fe-4S] cluster (Fig. 6e). Lastly, the estimation of iron
395 and sulfide ions in the native SufR revealed the association of 3.23-3.75-iron
396 atoms/SufR monomer and similar amounts of sulfide ion/SufR monomer (Fig.
397 6f). In sum, we demonstrate that *Mtb* SufR contains a 4Fe-4S cluster.

398

399 **SufR responds to NO through its 4Fe-4S cluster**

400 We exposed native SufR to the fast releasing NO donor; proline
401 NONOate ($T_{1/2}$ ~ 1.8 s, pH 7.4) and subjected it to UV-visible spectroscopy.

402 Treatment with proline NONOate gradually reduced absorbance at 413 nm
403 and formed a new chromophoric feature at ~ 350 nm over time with a clear
404 isosbestic point (Fig 7a). These spectral features are consistent with a
405 dinitrosyl-iron dithiol complex (DNIC), wherein the sulfide ligands of the 4Fe-
406 4S clusters are displaced by NO to form [Fe-$(NO)_2$] (52). The DNIC formation
407 was confirmed by subjecting NO-treated SufR to continuous wave Electron
408 Paramagnetic Resonance (cw-EPR). A strong EPR signal centered at *g*=2.03
409 was observed in a dose-dependent manner, consistent with the formation of
410 the monomeric DNIC complex on SufR (Fig. 7b) (18).

411

412 The *suf* operon showed induction under oxidizing stress (*e.g,* H_2O_2) (53).
413 Therefore, we determined whether the Fe-S cluster of SufR is responsive to
414 O_2 and H_2O_2. Exposure to atmospheric O_2 resulted in a slow decline in
415 absorbance at 413 nm (Fig. 7c). A plot of ΔA_{413nm} against time revealed the
416 loss of ~75% of the 4Fe-4S cluster only at 20 hr post-O_2 exposure. However,
417 exposure of native SufR to 1 mM H_2O_2 resulted in the rapid loss of absorption
418 at 413 nm (Fig. 7d). A plot of ΔA_{413nm} against time revealed the loss of ~75%
419 of the 4Fe-4S cluster in 20 min. Higher concentrations of H_2O_2 (10 mM and
420 100 mM) resulted in the loss of the cluster within 1-2 min (SI Appendix, Fig.
421 S9 a-c). Taken together, these data demonstrate that the 4Fe-4S cluster of
422 SufR is sensitive to NO and H_2O_2.

423

424 **SufR binds upstream of the *suf* operon promoter and represses**
425 **expression**

426 To investigate the DNA binding properties of SufR, we carried out
427 electrophoretic mobility shift assays (EMSA) using a radioactively (^{32}P)
428 labeled 170 bp DNA fragment encompassing the promoter region of *suf*
429 operon (23). We used four different forms of SufR; native/holo-SufR, apo-
430 SufR, NO-treated SufR, and H_2O_2-treated SufR. As shown in figure 8a, holo-
431 SufR binds to the *suf* promoter region in a concentration-dependent manner,
432 whereas apo-SufR, NO- treated SufR, and H_2O_2-treated SufR show no DNA
433 binding (Fig. 8a-c). Moreover, DNA binding was outcompeted by 50-100-fold
434 excess of unlabeled *suf* promoter DNA, but not by an unrelated promoter
435 fragment (*blaC*) (Fig. 8d). These findings suggest that *Mtb* SufR is an NO-
436 and H_2O_2-responsive, sequence-specific DNA binding protein.

437

438 We next performed *in vitro* transcription using *Mtb* RNA polymerase as
439 described (54). Single round of transcription of the *suf* promoter fragment (180
440 bp [-73 to + 107 bp]) produced a single transcript of 107 nucleotides,
441 consistent with the leaderless transcription of the *suf* operon (55). Addition of
442 holo-SufR represses transcription from the *suf* promoter in a dose-dependent
443 manner, whereas apo SufR does not (Fig. 8e-f). Importantly, the treatment of
444 native SufR with proline NONOate (NO) reversed the repression of *suf*
445 promoter (Fig. 8g). These results indicate that holo-SufR binds to the *suf*
446 promoter and represses expression, whereas NO-damaged or clusterless
447 apo-SufR lacks DNA binding and transcription repression. The data suggest
448 that occupancy of Fe-S cluster on SufR serves as an indicator of Fe-S cluster
449 sufficient or deficient conditions. During low Fe-S cluster demand, holo-SufR
450 represses the Suf system to reduce Fe-S cluster assembly, whereas loss or

451 damage of the Fe-S cluster in SufR signals heightened demand for Fe-S
452 clusters that results in the de-repression of the *suf* operon and mobilization of
453 Fe-S cluster assembly. In support of this, limiting Fe-S cluster biogenesis by
454 depleting SufT (CRIPSRi-*sufT*) alleviates the SufR-dependent repression of
455 the *suf* operon in *Mtb*, suggesting that *suf* machinery assembles the Fe-S
456 cluster on SufR to regulate Fe-S homeostasis (SI Appendix, Fig. S10).

457

458 Lastly, we performed DNase I footprinting to identify the binding site of
459 native SufR on the promoter region of the *suf* operon (Fig. 9). A clear region
460 of protection from DNase I digestion was evident with increasing molar ratios
461 of SufR:DNA (Fig. 9a-b). The protected region contains a perfect inverted
462 repeat (**ACACT**-N_5-**TGTGA)** that is separated by 5 bp (Fig. 9). This inverted
463 repeat forms a part of a larger inverted repeat (**ATTTT**GTCACACT-N_5-
464 TGTG**AAAAT**). Consistent with the footprinting data, mutations in the inverted
465 repeat completely abolished binding, thus confirming that the SufR binds the
466 palindrome **ACACT**-N_5-**TGTGA (Fig. 9c-e).** This palindromic sequence was
467 found to be present upstream of ~ 10 genes deregulated in *MtbΔsufR* under
468 NO stress (Data set S1E). Altogether, using multiple techniques we
469 confirmed that SufR functions as a NO- and H_2O_2-sensitive DNA-binding
470 transcription factor in *Mtb*.

471

472 **Discussion**

473 Fe-S cluster production is tightly regulated to promote Fe-S
474 formation when the necessity for the clusters is heightened (*e.g.,* ROI/RNI/iron

475 limitation) and to limit unnecessary production when the demand is low (*e.g.,*
476 hypoxia) (56). Deregulation of Fe-S cluster biogenesis can lead to toxic
477 accumulation of iron and polysulfides inside cells (56). Little is known about
478 how *Mtb* senses the need for Fe-S cluster biogenesis/regeneration in
479 response to ROI/RNI stress and the nature of the underlying regulatory
480 mechanisms. Here we show that *Mtb* SufR responds to one of the major
481 dormancy signals, NO, through its 4Fe-4S cluster. We provided biochemical
482 evidence that *Mtb* SufR contains a redox-responsive 4Fe-4S cluster that
483 reacts with NO. We also establish a link between NO, Fe-S biogenesis,
484 respiration, and SufR. Our findings provide a new mechanistic insight into how
485 *Mtb* exploits Fe-S cluster regulation and biogenesis processes under NO
486 stress to favor the pathogen's persistence.

487

488 Our RNA-seq data revealed a major realignment of expression of
489 genes encoding Fe-S cluster proteins and Fe-S cluster biogenesis (*suf*
490 operon) in NO-treated *Mtb*. Reduced expression of Fe-S cluster factors
491 associated with energy generation (*e.g.,* TCA cycle and primary respiration)
492 indicates that metabolic constraints imposed by NO represent the proximal
493 cause of growth arrest in *Mtb*. Moreover, while the majority Fe-S cluster
494 proteins are degraded in NO-stressed *Mtb* (13), Suf proteins remained
495 induced, suggesting that the *suf* operon is likely to facilitate regeneration of
496 Fe-S clusters during recovery from NO stress. This is reinforced by our data
497 showing an excellent recovery of Acn activity upon removal of NO stress in
498 case of wt *Mtb* but not in *MtbΔsufR* cells. Likewise, recovery from NO-
499 mediated growth arrest was significantly delayed in *MtbΔsufR*. Given the

500 strong reactivity of NO to metabolic and respiratory enzymes coordinating Fe-
501 S clusters and heme-Fe (25), we observed major changes in bacterial
502 OXPHOS, ECAR, and E_{MSH}, suggesting that NO-mediated cytostasis is
503 coupled to changes in redox balance and bioenergetics in *Mtb*. Our seahorse
504 XF flux data provide new insights into the mechanisms of NO-mediated
505 respiratory arrest in *Mtb*.

506

507 We discovered that under low electron (e^-) flux and high O_2
508 conditions (basal respiration), NO stimulated OCR possibly by collapsing
509 proton motive force (PMF). This is in agreement with the role of NO in
510 depolarizing the cytoplasmic membrane to arrest respiration and growth (57,
511 58). Upon artificially increasing the e^- flux through the respiratory chain (CCCP
512 treatment), which also depletes O_2 (59), NO efficiently inhibited O_2
513 consumption and depleted SRC of *Mtb*. In line with this, the transcriptome of
514 *Mtb* is remarkably responsive to NO under O_2 limitation (2). We also found
515 that spare respiratory capacity of *MtbΔsufR* is more severely inhibited by NO
516 as compared to wt *Mtb*. Since spare respiratory capacity depends mainly on
517 the recruitment of previously inactive respiratory complexes (60), the
518 sustained activation of the SUF system can provide a reserve of Fe-S cluster-
519 containing respiratory complexes to maintain electron transfer in response to
520 NO. Induction of the *suf* operon in response to conditions that damage Fe-S
521 clusters (*e.g.,* H_2O_2, NO, iron-starvation, antibiotics, phagosomal pH, and
522 sputum) (42, 53, 54, 61-64) indicates that *Mtb* relies on Suf-dependent Fe-S
523 cluster coordination to maintain persistence.

524

525 Our biochemical data support the role of SufR in sensing and
526 activating Fe-S cluster biogenesis under unfavorable conditions. For example,
527 H_2O_2 and NO rapidly targeted the 4Fe-4S cluster of SufR, whereas O_2 was
528 extremely sluggish. In agreement with this, Acn activity was largely unaffected
529 in *MtbΔsufR* under aerobic conditions but was significantly perturbed following
530 exposure to NO. Interestingly, a stand-alone *Mtb* cysteine desulfurase (IscS)
531 likely coordinates Fe-S clusters of Acn and succinate dehydrogenase under
532 aerobic conditions (65). Data suggest that *Mtb* prefers IscS for housekeeping
533 functions but the Suf system for managing stress. Similar roles were assigned
534 for IscS and Suf systems in *E. coli* (56). From the regulation perspective, SufR
535 appears to coordinate the expression of the *suf* operon in a negative feedback
536 loop. Holo-SufR serves as an indicator of Fe-S cluster sufficiency and
537 represses the *suf* operon, whereas apo- or DNIC forms of SufR indicate Fe-S
538 deficiency, resulting in derepression of the *suf* operon. Once the Fe-S cluster
539 demands are satisfied, the *suf* system reconstitutes the Fe-S cluster of SufR
540 to maintain homeostasis. We propose that this carefully choreographed
541 mechanism allows *Mtb* to calibrate Fe-S cluster supply with demand in
542 response to environmental signals encountered during infection, as shown
543 schematically in figure10.

544

545 The marginal survival defect of *MtbΔsufR* inside resting
546 macrophages and during early stages of infection *in vivo* indicates a lower
547 requirement of *suf*-dependent Fe-S biogenesis or possible compensation by
548 IscS. Consistent with this, *MtbΔsufR* showed attenuated phenotype inside the
549 nitrosatively hostile environment of activated macrophages and chronically

550 infected lung tissues. Both of these microenvironments are likely to increase
551 the demand for Fe-S cluster biogenesis. The capacity of SufR to sense and
552 respond to a range of cues, such as NO, H_2O_2, and iron limitation, possibly
553 empowers *Mtb* to transduce different redox signals into transcriptional
554 responses crucial for persistence *in vivo*. The overexpression of the DosR
555 regulon in *MtbΔsufR* relative to wt *Mtb* specifically under NO stress indicates
556 that SufR-mediated gene regulation extends beyond derepression of the *suf*
557 operon. Interestingly, the *suf* operon was overexpressed in *MtbΔdosR* under
558 hypoxia (15), signifying a regulatory loop between SufR and DosR in *Mtb*.
559 This is supported by our *in vivo* data wherein the persistence defect displayed
560 by *MtbΔsufR* was partially restored in *sufR*-Comp even though the expression
561 of the *suf* operon was not reinstated. Interestingly, the expression of the DosR
562 regulon recovered to wt levels in *sufR*-Comp, suggesting that further work is
563 required to explore the breadth of SufR-mediated gene regulation. Based on
564 this cumulative evidence, we propose that *Mtb* SufR senses NO through its Fe-S
565 cluster to coordinate Fe-S cluster biogenesis and regulate metabolism,
566 respiration, and redox balance for long-term persistence.

567

568 **Methods:**

569 **Culture Conditions**. The *Mtb* H37Rv, *MtbΔsufR,* and *sufR*-comp
570 were grown in Middlebrook 7H9 broth (Becton, Dickinson and Company (BD),
571 USA) medium supplemented with 0.2% glycerol, 0.5% BSA, 0.2% dextrose,
572 and 0.085% NaCl (ADS) with 0.05% Tween 80 as described previously (42).
573 For culturing on solid medium, *Mtb* strains were cultured on 7H10/7H11 agar
574 medium (Becton, Dickinson and Company (BD), USA) supplemented with 1x

575 OADC (Becton, Dickinson and Company (BD), USA) and 0.2% glycerol. *E.*
576 *coli* cultures were grown in LB medium (HIMEDIA, India). Whenever required,
577 antibiotics were added to the culture medium (for *E. coli*, 100 µg/ml
578 kanamycin (Amresco, USA) and 150 µg/ml hygromycin (Sigma-Aldrich, India);
579 for *Mtb* strains, 50 µg/ml hygromycin).

580

581 **RNA Sequencing experiments**:

582 The *Mtb* strains were grown to an $O.D._{600}$ of 0.4 and exposed to 0.5
583 mM diethylenetriamine-nitric oxide (DETA/NO [Sigma-Aldrich, India]) for 4 h at
584 $37^{o}C$. The experiment was carried out with three independent biological
585 replicates. Total RNA extraction was conducted using the FastRNA® Pro Blue
586 Kit (MP Biomedicals, USA) in accordance with the manufacturer's instruction
587 and further purified using RNeasy spin columns (Qiagen, USA) as described
588 (42). Following purification, the RNA was quantified and assessed for purity
589 by a 2100 Bioanalyzer (Agilent Technologies, Waldbronn, Germany). RNA
590 samples with an RIN (RNA Integrity Number) value >8 were processed further
591 for sequencing. Ribosomal RNA (16s and 23s rRNA) was removed by
592 hybridization with magnetic beads-coupled oligonucleotide (MicrobExpress
593 Kit, Life Technologies, USA) and concentration of enriched mRNA was
594 quantified by QuBit RNA HS Assay Kit (Life Technologies, USA). RNA-seq
595 was performed as described (17). In brief, libraries were prepared using
596 NEBNextUltra Directional RNA Library Prep Kit for Illumina' (New England
597 Biolabs, USA), according to manufacturer's instructions. The library size
598 distribution and quality were assessed using a high sensitivity DNA Chip
599 (Agilent Technologies, USA) and sequenced in HiSeq 2500 platform (Illumina,

600 USA) sequencer using 1X50 bp single-end reads with 1% PhiX spike-in
601 control. All the raw data were deposited into the NCBI Gene Expression
602 Omnibus (GEO)
603 (https://www.ncbi.nlm.nih.gov/geo/query/acc.cgi?acc=GSE154169 with the
604 accession number GSE154169 and reviewer token kbcdmqecrlotzgp.

605

606 **Differential gene expression and statistical analysis for RNA-Seq:**

607 Raw reads were obtained for *Mtb* H37Rv strain as fastq files. The
608 reference genome sequence (.fna) and annotation (.gff) files for the same
609 strain (accession number: NC_000962.3) were downloaded from the ncbi ftp
610 website ("ftp.ncbi.nlm.nih.gov"). The annotation file was customized with the
611 addition of annotations for non-coding RNAs (66). The format of the
612 annotation file (.gff) was changed to .bed using an in-house python script. The
613 raw read quality was checked using the FastQC software (version v0.11.5;
614 http://www.bioinformatics.babraham.ac.uk/projects/fastqc). BWA (version
615 0.7.12-r1039)(67) was used to index the reference genome. Reads with raw
616 read quality >= 20 were aligned using BWA aln -q option. SAMTOOLS
617 (version 0.1.19-96b5f2294a) (68) was used to filter out the multiply mapped
618 reads. BEDTOOLS (version 2.25.0)(69) was used to calculate the reads count
619 per gene using the annotation file (.bed). The normalization and differential
620 gene expression analysis for the conditions were carried out using edgeR as
621 mentioned previously (70). Genes with at least 10 reads were selected for
622 each comparative analysis. DGE analysis was done in RStudio (1.1.447) with
623 R version 3.4.4. (*http://www.rstudio.com/*)

624

625 **Aconitase assay:**

626 The activity of aconitase (Acn) was measured by monitoring the
627 disappearance of cis-aconitate at 240nm in a UV spectrophotometer (Thermo
628 Scientific Biomat 3S, USA) as described (71). One unit (U) of aconitase
629 activity is defined as 1μmol cis-aconitate formed or converted per minute.
630 Reaction mixtures (1ml) for Acn contained 25mM Tris-HCl (pH 8.0), 100 mM
631 NaCl, and 50 μg *Mtb* cell lysates. Reactions were initiated by adding 0.15 mM
632 cis-aconitate and monitored by following the disappearance of cis-aconitate at
633 240 nm after every 15 sec for total 30 min. Absorbance at 240 was plotted
634 against time. Acn activity was calculated from linear portion of the curve in
635 initial 5 min when reaction follows 0th order of reaction. An extinction
636 coefficient of 3,500 $M^{-1}cm^{-1}$ was used to calculate the rates.

637

638 **OCR and ECAR measurements:**

639 The *Mtb* strains adhered to the bottom of a XF cell culture
640 microplate (Agilent technologies, USA), at $2X10^6$ bacilli per well by using Cell-
641 Tak (a cell adhesive). OCR and ECAR were measured using Agilent XF
642 Extracellular Flux Analyser. Assays were carried out in unbuffered 7H9 media
643 (pH 7.35) with glucose 2mg/ml as carbon source. Basal OCR and ECAR were
644 measured for initial 21 min before the automatic addition of freshly prepared
645 DETA-NO (0 mM, 0.25 mM, 0.5 mM and 1 mM) in 7H9 unbuffered media,
646 through port A of cartridge plate. Three measurements were taken after 1 h of
647 incubation. CCCP (Sigma-Aldrich, India) was added at 10 μM concentration to
648 achieve maximum rate of respiration. Raw data of OCR and ECAR was CFU

649 normalised for $2X10^6$ CFU/ well. Spare respiratory capacity, was calculated
650 from % OCR value, by subtracting third basal reading (normalized as 100%)
651 from first point after CCCP addition.

652

653 **Animal experiments:**

654 For the chronic model of infection, 5- to 6-week-old female
655 BALB/c, C57BL/6 and $iNOS^{-/-}$ mice (n = 6 per group) were infected by aerosol
656 with approximately 100 bacilli per mouse with the *Mtb* strains using a Madison
657 chamber aerosol generation. At indicated times post infection, mice were
658 euthanized, and the lungs were harvested for bacillary load, tissue
659 histopathology analysis, and pathological scoring as described (42). The
660 remaining tissue samples from each mouse were homogenized and bacillary
661 load was quantified by plating serial dilutions of tissue homogenates onto
662 Middlebrook 7H11-OADC agar plates supplemented with lyophilized BBL
663 MGIT PANTA antibiotic mixture ((polymyxin B, amphotericin B, nalidixic acid,
664 trimethoprim, and azlocillin, as supplied by BD;USA). Colonies were observed
665 and counted after 4 weeks of incubation at 37°C.

666

667 **EPR spectroscopy of SufR:**

668 For EPR spectroscopy, Holo SufR was treated inside the
669 anaerobic glove box with aliquots of freshly prepared proline NONOate
670 (Cayman Chemicals, Ann Arbor, MI, USA). Aliquots of SufR were placed in an
671 anaerobic cuvette and titrated by injection with aliquots of a 2.5 mM stock
672 solution of proline NONOate (Cayman chemicals, USA). Samples were then

673 transferred to EPR tubes and immediately frozen in liquid nitrogen. EPR
674 characteristics of NO-treated SufR were analyzed by subjecting the samples
675 to continuous-wave spectrometers at liquid nitrogen temperature as described
676 previously (18). NO-treated SufR was analyzed by continuous-wave EPR on a
677 perpendicular mode X-band EPR spectrometer operating at 100-kHz
678 modulation frequency and equipped with liquid nitrogen cryostat and a dual
679 mode X-band cavity (JES200 ESR spectrometer, JEOL, USA). Field
680 calibration was done by using a standard NMR G meter. The background
681 signal from the buffer was subtracted from the spectra.

682

683 **Electrophoretic mobility shift assays (EMSA):**

684 For EMSA promoter fragment of *sufR* (170 bp upstream of ATG)
685 and *blaC* (200 bp upstream of ATG) were PCR amplified from the *Mtb*
686 genome. The 5' end was labeled by [Y-32_P]-ATP using T4 polynucleotide
687 kinase (MBI Fermentas, USA) as per the manufacturer's instructions. The
688 labeled oligonucleotides were passed through a 1 mL Tris-EDTA, pH 7.5
689 equilibrated Sephadex G-50 column and elute was vacuum dried. Blunt ended
690 duplex DNA was prepared by annealing radiolabelled and complementary
691 cold oligonucleotides in a 1: 2 molar ratio in 50 µL reaction system containing
692 TE and 1X saline-sodium citrate buffer (3 M sodium chloride and 0.3 M
693 sodium citrate). The reaction mixture was heated to 95 °C for 5 min and then
694 cooled in a thermal cycler. Annealed mixtures were resolved by 10% native
695 PAGE in 1x Tris-borate EDTA (TBE). Assembled DNA substrates were
696 visualized on an X-ray film and substrates were subsequently purified by
697 excising the respective desired bands. DNA substrates were eluted by

698 incubating corresponding gel pieces in TE at 4°C for 6 h. Binding reactions
699 were performed in Binding buffer (25mM Tris-HCl, 1mM DTT, 0.1 mg/ml BSA,
700 5 mM $MgCl_2$; pH 7.4) for 30 min at 4°C and 6% polyacrylamide gel was used
701 to resolve protein-DNA complexes in an anaerobic chamber by
702 electrophoresis at constant voltage (50 V). 0.5 nM ^{32}P-labeled DNA substrates
703 were incubated with indicated concentrations of various forms of SufR (apo-,
704 holo-, H_2O_2-treated, and NO-treated). For competition with unlabeled DNA,
705 fragments of *sufR* and *blaC* (~200–250 bp upstream of translational start
706 codon) were PCR amplified from the *Mtb* genome and used in various
707 amounts to outcompete binding of holo-SufR to ^{32}P-labelled DNA fragments.
708 Gels were exposed to auto radiographic film and visualized by a phosphor
709 imager (Typhoon FLA-9000, GE Healthcare Life Sciences, USA). All the
710 above reaction and separation were performed under anaerobic condition
711 inside glove box (Plas-Labs, Lansing, MI, USA).

712

713 **DNase I Footprinting :**

714 Five nanomolar of ^{32}P-labeled DNA substrate was incubated with
715 increasing concentration of purified holo-SufR in binding buffer (25 mM Tris-
716 HCl (pH 7.5), 1mM DTT, 100 µg/ml BSA, 5 mM MgCl2, 5 mM CaCl2), and
717 samples were incubated for 30 min at 4 °C inside glove box under anaerobic
718 condition. Reactions were initiated by the addition of DNase I to a final
719 concentration of 0.05 units and incubated for 2 min at room temperature. The
720 reactions were terminated by the addition of 150µL of TE (pH 7.5) followed by
721 incubation at 75°C for 15 mins to deactivate DNase I enzyme. The sample
722 was further subjected to vacuum evaporation and the pellet thus obtained was

723 re-suspended in loading dye (80% (v/v) formamide, 0.1% (v/v) BPB, and 0.1%
724 (v/v) xylene cyanol) and analyzed on a denaturing 15% polyacrylamide gel
725 containing 7M urea. The gel was dried, and the bands were visualized with a
726 Typhoon FLA-9000 phosphor imager (GE Healthcare Life Sciences, USA).
727 Maxam and Gilbert A + G ladder was prepared as described previously (72).

728 A custom python script was developed to search for the SufR binding site and
729 find its relative positions with respect to genes across the genome. A
730 sequence of 15 nt length was searched in the region 500 bp upstream of the
731 start codon and considered as a potential SufR binding site if it shares 80%
732 identity with 'ACACT' or 'TGTGA' at the ends.

733

734 **Supplementary methods:**

735 Please refer to supplementary (SI) appendix section for western
736 blotting, cellRox deep staining and flow cytometry, construction of *Mtb* SufT
737 Knock Down strain, NO exposure and recovery, cell line infection
738 experiments, purification of SufR under anaerobic conditions, UV-Vis, CD
739 analysis, and gel filtration of SufR, chemical analysis of Iron and Sulfide, and
740 *In vitro* transcription assays.

741

742 **Ethics:**

743 Animal experimentation: This study was carried out in strict accordance with
744 the guidelines provided by the Committee for the Purpose of Control and
745 Supervision on Experiments on Animals (CPCSEA), Government of India.
746 The protocol of animal experiment was approved by animal ethical Committee

747 on the Ethics of Animal Experiments, Indian Institute of science (IISc),
748 Bangalore, India (Approval number: CAF/Ethics/544/2017). All efforts were
749 made to minimize the suffering.

750

751 **Acknowledgements:**

752 We are thankful to Next Generation Genomics Facility (NGGF) at National
753 Centre for Biological Sciences, Bangalore, for conducting the RNA
754 sequencing. We thank BSL3 facilities at CIDR, IISc Bangalore. We thank A.
755 Varalakshmi (Sophisticated Analytical Instrument Facility, IIT Chennai, India)
756 for excellent technical help In EPR experiments. The *Mtb* work was supported
757 by the following Wellcome Trust/DBT India Alliance Grants, IA/S/16/2/502700
758 (AS), IA/E/16/1/503017 (KA), and in part by Department of Biotechnology
759 (DBT) Grant BT/PR11911/BRB/10/1327/2014,
760 BT/PR5020/MED/29/1454/2012 (AS) and DBT-IISc Partnership Program (22-
761 0905-0006-05-987-436). AS and KA are senior- and early- career fellows of
762 Wellcome Trust/DBT India Alliance.

763

764 **Author contributions:**

765 KA, AT, and AS participated in the design of the study. KA, AT, KS, NM, AJ,
766 RKJ, RSR, and, SNC, carried out the experiments. AR, VN, BG, GN, and
767 ASN contributed to reagents and analyzed the data. KA and AS conceived the
768 study, supervised the project, analyzed the data and drafted the manuscript.
769 All authors read and approved the final manuscript.

770

771 **Conflict of interest statement:**

772 The authors have no conflict of interests to declare.

773

774 **References**

775 1. Mishra BB*, et al.* (2013) Nitric oxide controls the immunopathology of
776 tuberculosis by inhibiting NLRP3 inflammasome-dependent processing
777 of IL-1beta. *Nat Immunol* 14(1):52-60.
778 2. Voskuil MI*, et al.* (2003) Inhibition of respiration by nitric oxide induces
779 a *Mycobacterium tuberculosis* dormancy program. *J Exp Med*
780 198(5):705-713.
781 3. Nathan C & Shiloh MU (2000) Reactive oxygen and nitrogen
782 intermediates in the relationship between mammalian hosts and
783 microbial pathogens. *Proc Natl Acad Sci U S A* 97(16):8841-8848.
784 4. MacMicking J, Xie QW, & Nathan C (1997) Nitric oxide and
785 macrophage function. *Annual review of immunology* 15:323-350.
786 5. MacMicking JD*, et al.* (1997) Identification of nitric oxide synthase as a
787 protective locus against tuberculosis. *Proc Natl Acad Sci U S A*
788 94(10):5243-5248.
789 6. Nicholson S*, et al.* (1996) Inducible nitric oxide synthase in pulmonary
790 alveolar macrophages from patients with tuberculosis. *J Exp Med*
791 183(5):2293-2302.
792 7. Mattila JT*, et al.* (2013) Microenvironments in tuberculous granulomas
793 are delineated by distinct populations of macrophage subsets and
794 expression of nitric oxide synthase and arginase isoforms. *J Immunol*
795 191(2):773-784.
796 8. Wang CH*, et al.* (1998) Increased exhaled nitric oxide in active
797 pulmonary tuberculosis due to inducible NO synthase upregulation in
798 alveolar macrophages. *Eur Respir J* 11(4):809-815.
799 9. Schon T*, et al.* (2003) Arginine as an adjuvant to chemotherapy
800 improves clinical outcome in active tuberculosis. *Eur Respir J*
801 21(3):483-488.
802 10. Schon T*, et al.* (2011) Effects of a food supplement rich in arginine in
803 patients with smear positive pulmonary tuberculosis--a randomised
804 trial. *Tuberculosis (Edinb)* 91(5):370-377.
805 11. Kumar A, Toledo JC, Patel RP, Lancaster JR, Jr., & Steyn AJ (2007)
806 *Mycobacterium tuberculosis* DosS is a redox sensor and DosT is a
807 hypoxia sensor. *Proc Natl Acad Sci U S A* 104(28):11568-11573.
808 12. Sardiwal S*, et al.* (2005) A GAF domain in the hypoxia/NO-inducible
809 *Mycobacterium tuberculosis* DosS protein binds haem. *J Mol Biol*
810 353(5):929-936.
811 13. Cortes T*, et al.* (2017) Delayed effects of transcriptional responses in
812 *Mycobacterium tuberculosis* exposed to nitric oxide suggest other
813 mechanisms involved in survival. *Sci Rep* 7(1):8208.

814 14. Shiloh MU, Manzanillo P, & Cox JS (2008) *Mycobacterium tuberculosis*
815 senses host-derived carbon monoxide during macrophage infection.
816 *Cell Host Microbe* 3(5):323-330.
817 15. Park HD*, et al.* (2003) Rv3133c/dosR is a transcription factor that
818 mediates the hypoxic response of *Mycobacterium tuberculosis*. *Mol*
819 *Microbiol* 48(3):833-843.
820 16. Chinta KC*, et al.* (2016) The emerging role of gasotransmitters in the
821 pathogenesis of tuberculosis. *Nitric Oxide* 59:28-41.
822 17. Huet G, Daffe M, & Saves I (2005) Identification of the *Mycobacterium*
823 *tuberculosis* SUF machinery as the exclusive mycobacterial system of
824 [Fe-S] cluster assembly: evidence for its implication in the pathogen's
825 survival. *J Bacteriol* 187(17):6137-6146.
826 18. Singh A*, et al.* (2007) *Mycobacterium tuberculosis* WhiB3 responds to
827 O2 and nitric oxide via its [4Fe-4S] cluster and is essential for nutrient
828 starvation survival. *Proc Natl Acad Sci U S A* 104(28):11562-11567.
829 19. Mehta M & Singh A (2019) *Mycobacterium tuberculosis* WhiB3
830 maintains redox homeostasis and survival in response to reactive
831 oxygen and nitrogen species. *Free Radic Biol Med* 131:50-58.
832 20. Kudhair BK*, et al.* (2017) Structure of a Wbl protein and implications for
833 NO sensing by *M. tuberculosis. Nature communications* 8(1):2280.
834 21. Hickok JR*, et al.* (2011) Dinitrosyliron complexes are the most
835 abundant nitric oxide-derived cellular adduct: biological parameters of
836 assembly and disappearance. *Free Radic Biol Med* 51(8):1558-1566.
837 22. Pandey M, Talwar S, Bose S, & Pandey AK (2018) Iron homeostasis in
838 *Mycobacterium tuberculosis* is essential for persistence. *Sci Rep*
839 8(1):17359.
840 23. Willemse D*, et al.* (2018) Rv1460, a SufR homologue, is a repressor of
841 the suf operon in *Mycobacterium tuberculosis*. *PLoS One*
842 13(7):e0200145.
843 24. Fang FC (2004) Antimicrobial reactive oxygen and nitrogen species:
844 concepts and controversies. *Nat Rev Microbiol* 2(10):820-832.
845 25. Cooper CE (1999) Nitric oxide and iron proteins. *Biochim Biophys Acta*
846 1411(2-3):290-309.
847 26. Crack JC, Green J, Thomson AJ, & Le Brun NE (2014) Iron-sulfur
848 clusters as biological sensors: the chemistry of reactions with
849 molecular oxygen and nitric oxide. *Acc Chem Res* 47(10):3196-3205.
850 27. Cook GM, Hards K, Vilcheze C, Hartman T, & Berney M (2014)
851 Energetics of Respiration and Oxidative Phosphorylation in
852 Mycobacteria. *Microbiol Spectr* 2(3).
853 28. Baughn AD, Garforth SJ, Vilcheze C, & Jacobs WR, Jr. (2009) An
854 anaerobic-type alpha-ketoglutarate ferredoxin oxidoreductase
855 completes the oxidative tricarboxylic acid cycle of *Mycobacterium*
856 *tuberculosis*. *PLoS pathogens* 5(11):e1000662.
857 29. Palde PB*, et al.* (2016) First-in-Class Inhibitors of Sulfur Metabolism
858 with Bactericidal Activity against Non-Replicating M. tuberculosis. *ACS*
859 *chemical biology* 11(1):172-184.
860 30. Boshoff HI*, et al.* (2008) Biosynthesis and recycling of nicotinamide
861 cofactors in *Mycobacterium tuberculosis*. An essential role for NAD in
862 nonreplicating bacilli. *The Journal of biological chemistry*
863 283(28):19329-19341.

31. Buchko GW, Hewitt SN, Napuli AJ, Van Voorhis WC, & Myler PJ (2011) Solution-state NMR structure and biophysical characterization of zinc-substituted rubredoxin B (Rv3250c) from *Mycobacterium tuberculosis*. *Acta Crystallogr Sect F Struct Biol Cryst Commun* 67(Pt 9):1148-1153.
32. Harper AE, Miller RH, & Block KP (1984) Branched-chain amino acid metabolism. *Annu Rev Nutr* 4:409-454.
33. Munoz-Elias EJ & McKinney JD (2006) Carbon metabolism of intracellular bacteria. *Cell Microbiol* 8(1):10-22.
34. Beites T*, et al.* (2019) Plasticity of the *Mycobacterium tuberculosis* respiratory chain and its impact on tuberculosis drug development. *Nature communications* 10(1):4970.
35. Brown AC, Eberl M, Crick DC, Jomaa H, & Parish T (2010) The nonmevalonate pathway of isoprenoid biosynthesis in *Mycobacterium tuberculosis* is essential and transcriptionally regulated by Dxs. *J Bacteriol* 192(9):2424-2433.
36. Ren B, Zhang N, Yang J, & Ding H (2008) Nitric oxide-induced bacteriostasis and modification of iron-sulphur proteins in *Escherichia coli*. *Mol Microbiol* 70(4):953-964.
37. Tortora V, Quijano C, Freeman B, Radi R, & Castro L (2007) Mitochondrial aconitase reaction with nitric oxide, S-nitrosoglutathione, and peroxynitrite: mechanisms and relative contributions to aconitase inactivation. *Free Radic Biol Med* 42(7):1075-1088.
38. Lill R (2009) Function and biogenesis of iron-sulphur proteins. *Nature* 460(7257):831-838.
39. Zhang J & Zhang Q (2019) Using Seahorse Machine to Measure OCR and ECAR in Cancer Cells. *Methods Mol Biol* 1928:353-363.
40. Dranka BP, Hill BG, & Darley-Usmar VM (2010) Mitochondrial reserve capacity in endothelial cells: The impact of nitric oxide and reactive oxygen species. *Free Radic Biol Med* 48(7):905-914.
41. Bhaskar A*, et al.* (2014) Reengineering redox sensitive GFP to measure mycothiol redox potential of *Mycobacterium tuberculosis* during infection. *PLoS pathogens* 10(1):e1003902.
42. Mishra R*, et al.* (2019) Targeting redox heterogeneity to counteract drug tolerance in replicating *Mycobacterium tuberculosis*. *Sci Transl Med* 11(518).
43. Li Y & He ZG (2012) The mycobacterial LysR-type regulator OxyS responds to oxidative stress and negatively regulates expression of the catalase-peroxidase gene. *PLoS One* 7(1):e30186.
44. Gomez RL*, et al.* (2016) The multiple stress responsive transcriptional regulator Rv3334 of *Mycobacterium tuberculosis* is an autorepressor and a positive regulator of kstR. *FEBS J* 283(16):3056-3071.
45. Smith LJ*, et al.* (2010) *Mycobacterium tuberculosis* WhiB1 is an essential DNA-binding protein with a nitric oxide-sensitive iron-sulfur cluster. *The Biochemical journal* 432(3):417-427.
46. Leistikow RL*, et al.* (2010) The *Mycobacterium tuberculosis* DosR regulon assists in metabolic homeostasis and enables rapid recovery from nonrespiring dormancy. *J Bacteriol* 192(6):1662-1670.

912 47. Tamuhla T, Joubert L, Willemse D, & Williams MJ (2020) SufT is
913 required for growth of *Mycobacterium smegmatis* under iron limiting
914 conditions. *Microbiology* 166(3):296-305.
915 48. MacMicking JD, Taylor GA, & McKinney JD (2003) Immune control of
916 tuberculosis by IFN-gamma-inducible LRG-47. *Science* 302(5645):654-
917 659.
918 49. Crack JC*, et al.* (2009) Characterization of [4Fe-4S]-containing and
919 cluster-free forms of Streptomyces WhiD. *Biochemistry* 48(51):12252-
920 12264.
921 50. Imlay JA (2006) Iron-sulphur clusters and the problem with oxygen. *Mol*
922 *Microbiol* 59(4):1073-1082.
923 51. Freibert SA*, et al.* (2018) Biochemical Reconstitution and
924 Spectroscopic Analysis of Iron-Sulfur Proteins. *Methods Enzymol*
925 599:197-226.
926 52. Cruz-Ramos H*, et al.* (2002) NO sensing by FNR: regulation of the
927 Escherichia coli NO-detoxifying flavohaemoglobin, Hmp. *EMBO J*
928 21(13):3235-3244.
929 53. Voskuil MI, Bartek IL, Visconti K, & Schoolnik GK (2011) The response
930 of *Mycobacterium tuberculosis* to reactive oxygen and nitrogen
931 species. *Front Microbiol* 2:105.
932 54. Mishra S*, et al.* (2017) Efficacy of beta-lactam/beta-lactamase inhibitor
933 combination is linked to WhiB4-mediated changes in redox physiology
934 of Mycobacterium tuberculosis. *Elife* 6.
935 55. Cortes T*, et al.* (2013) Genome-wide mapping of transcriptional start
936 sites defines an extensive leaderless transcriptome in *Mycobacterium*
937 *tuberculosis. Cell Rep* 5(4):1121-1131.
938 56. Mettert EL & Kiley PJ (2015) How Is Fe-S Cluster Formation
939 Regulated? *Annu Rev Microbiol* 69:505-526.
940 57. Jones-Carson J*, et al.* (2020) Nitric oxide disrupts bacterial cytokinesis
941 by poisoning purine metabolism. *Sci Adv* 6(9):eaaz0260.
942 58. Jones-Carson J*, et al.* (2014) Nitric oxide from IFNgamma-primed
943 macrophages modulates the antimicrobial activity of beta-lactams
944 against the intracellular pathogens Burkholderia pseudomallei and
945 Nontyphoidal Salmonella. *PLoS Negl Trop Dis* 8(8):e3079.
946 59. Jash S & Adhya S (2015) Effects of Transient Hypoxia versus
947 Prolonged Hypoxia on Satellite Cell Proliferation and Differentiation In
948 Vivo. *Stem Cells Int* 2015:961307.
949 60. Desler C*, et al.* (2012) Is There a Link between Mitochondrial Reserve
950 Respiratory Capacity and Aging? *J Aging Res* 2012:192503.
951 61. Tyagi P, Dharmaraja AT, Bhaskar A, Chakrapani H, & Singh A (2015)
952 *Mycobacterium tuberculosis* has diminished capacity to counteract
953 redox stress induced by elevated levels of endogenous superoxide.
954 *Free Radic Biol Med* 84:344-354.
955 62. Kurthkoti K*, et al.* (2017) The Capacity of *Mycobacterium tuberculosis*
956 To Survive Iron Starvation Might Enable It To Persist in Iron-Deprived
957 Microenvironments of Human Granulomas. *mBio* 8(4).
958 63. Van den Bossche A*, et al.* (2019) Transcriptional profiling of a
959 laboratory and clinical *Mycobacterium tuberculosis* strain suggests
960 respiratory poisoning upon exposure to delamanid. *Tuberculosis*
961 *(Edinb)* 117:18-23.

64. Kumar M, *et al.* (2011) Identification of *Mycobacterium tuberculosis* genes preferentially expressed during human infection. *Microb Pathog* 50(1):31-38.
65. Rybniker J, *et al.* (2014) The cysteine desulfurase IscS of *Mycobacterium tuberculosis* is involved in iron-sulfur cluster biogenesis and oxidative stress defence. *The Biochemical journal* 459(3):467-478.
66. Gerrick ER, *et al.* (2018) Small RNA profiling in *Mycobacterium tuberculosis* identifies MrsI as necessary for an anticipatory iron sparing response. *Proc Natl Acad Sci U S A* 115(25):6464-6469.
67. Li H & Durbin R (2009) Fast and accurate short read alignment with Burrows-Wheeler transform. *Bioinformatics* 25(14):1754-1760.
68. Li H, *et al.* (2009) The Sequence Alignment/Map format and SAMtools. *Bioinformatics* 25(16):2078-2079.
69. Quinlan AR & Hall IM (2010) BEDTools: a flexible suite of utilities for comparing genomic features. *Bioinformatics* 26(6):841-842.
70. Robinson MD, McCarthy DJ, & Smyth GK (2010) edgeR: a Bioconductor package for differential expression analysis of digital gene expression data. *Bioinformatics* 26(1):139-140.
71. Tian J, Bryk R, Itoh M, Suematsu M, & Nathan C (2005) Variant tricarboxylic acid cycle in *Mycobacterium tuberculosis*: identification of alpha-ketoglutarate decarboxylase. *Proc Natl Acad Sci U S A* 102(30):10670-10675.
72. Maxam AM & Gilbert W (1980) Sequencing end-labeled DNA with base-specific chemical cleavages. *Methods Enzymol* 65(1):499-560.

1008 **Figures with legends:**

1009

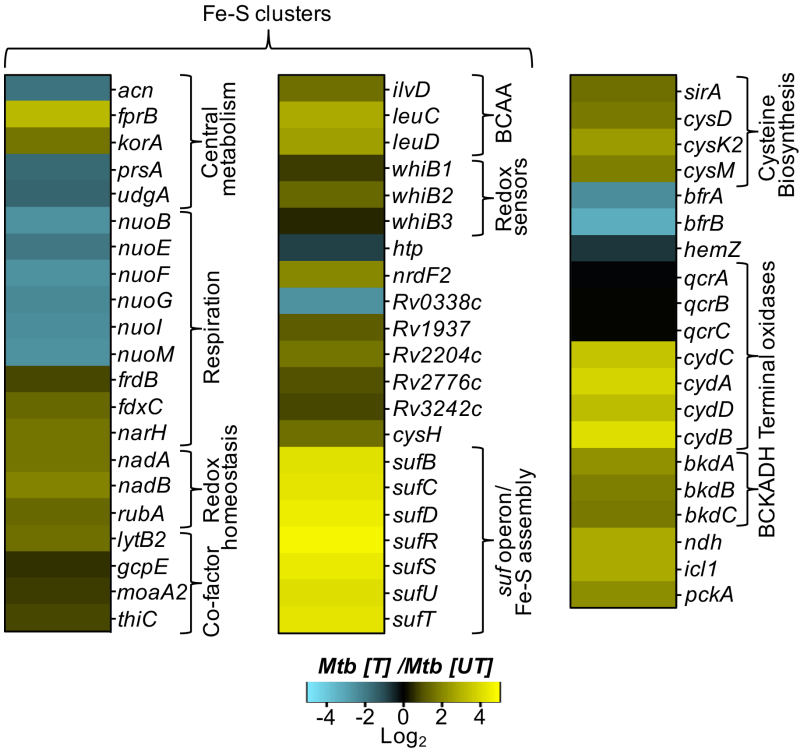

1010

1011 **Figure 1: Nitric oxide (NO) impacts Fe-S cluster transcriptome of *Mtb*.**
1012 Exponentially grown *Mtb* $H_{37}Rv$ was exposed to 0.5 mM DETA-NO for 4h in
1013 three biological replicates. Total RNA was isolated from untreated (UT) and
1014 DETA-NO treated (T) *Mtb* and subjected to RNA-seq analysis. Heat maps
1015 indicate log2 fold changes of differentially expressed genes (DEGs) belonging
1016 to various functional categories (obtained from Mycobrowser, EPFL,
1017 Lausanne). Genes were considered differentially expressed on the basis of
1018 the false discovery rate (FDR) of ≤0.05 and absolute fold change of ≥1.5.
1019 *BCCA: branched chain amino acid; BCKADH: branched chain keto-acid*
1020 *dehydrogenase complex*.

1021

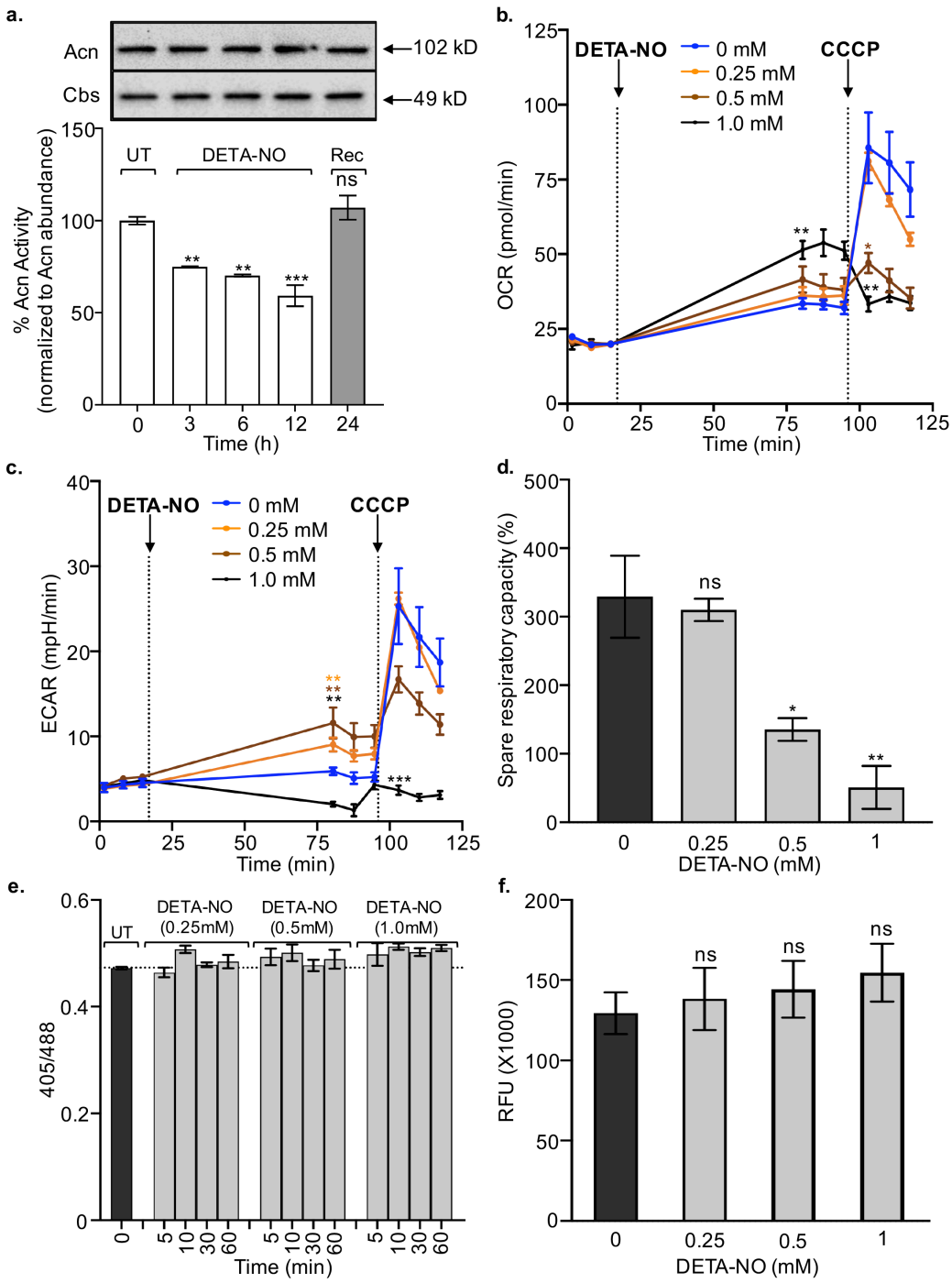

Figure 2: NO affects Fe-S homeostasis and bioenergetics of *Mtb*. a) Gradual reduction of aconitase (Acn) activity in response to 0.5 mM DETA-NO over time. At 12 h post-treatment, *Mtb* was cultured in a DETA-NO free 7H9 broth for 24h and recovery (Rec) of Acn activity was quantified as a measure of Fe-S cluster regeneration. Under these conditions, intracellular levels of Acn remained unaltered. A non Fe-S cluster protein cystathione-β-synthase

1029 (Cbs) of *Mtb* was used as an internal loading control. **b)** A change in Oxygen
1030 Consumption Rate (OCR) was quantified upon addition of indicated
1031 concentrations of DETA-NO by Seahorse XF flux analyser. The uncoupler
1032 CCCP was used to maximally induce respiration and to determine the
1033 influence of NO on the spare respiratory capacity (SRC). The first and second
1034 vertical lines indicate the point of addition of DETA-NO and CCCP,
1035 respectively. **c)** Extracellular Acidification Rate (ECAR) of DETA-NO treated
1036 *Mtb*. **d)** Decrease in SRC of *Mtb* with increasing concentrations of DETA-NO.
1037 Percentage SRC was calculated by subtracting basal OCR (before adding
1038 DETA-NO) to CCCP induced OCR considering basal OCR as 100%. **e**) *Mtb*
1039 expressing Mrx1-roGFP2 was exposed to the indicated concentrations of
1040 DETA-NO and changes in the biosensor ratio (405/488 nm) were measured
1041 using flowcytometer. **f)** *Mtb* treated with the indicated concentrations of DETA-
1042 NO for 2 h was stained with CellRox Deep Red reagent to measure
1043 endogenous ROS. Results are expressed as Mean ± SD. One-way analysis of
1044 variance (ANOVA) with Bonferroni's post hoc test was employed to determine
1045 statistical significance between different doses of DETA-NO. Data shown are
1046 the result of three independent experiments performed in triplicate. *p* value is
1047 <0.05 were indicated with symbols. Symbols: (*): comparison to untreated *Mtb*
1048 control. Statistical significance for the OCR and ECAR was obtained by
1049 comparing different doses of DETA-NO with untreated, Comparisons whose P
1050 value is <0.05 were indicated with different symbols. Symbols: (*): comparison
1051 to 0.25mM; (*): comparison to 0.5mM; and (*): comparison to 1.0 mM */*/*
1052 p<0.05; **/**/** p<0.01; ***/***/*** p<0.001. ns, no significant difference (P >
1053 0.05).

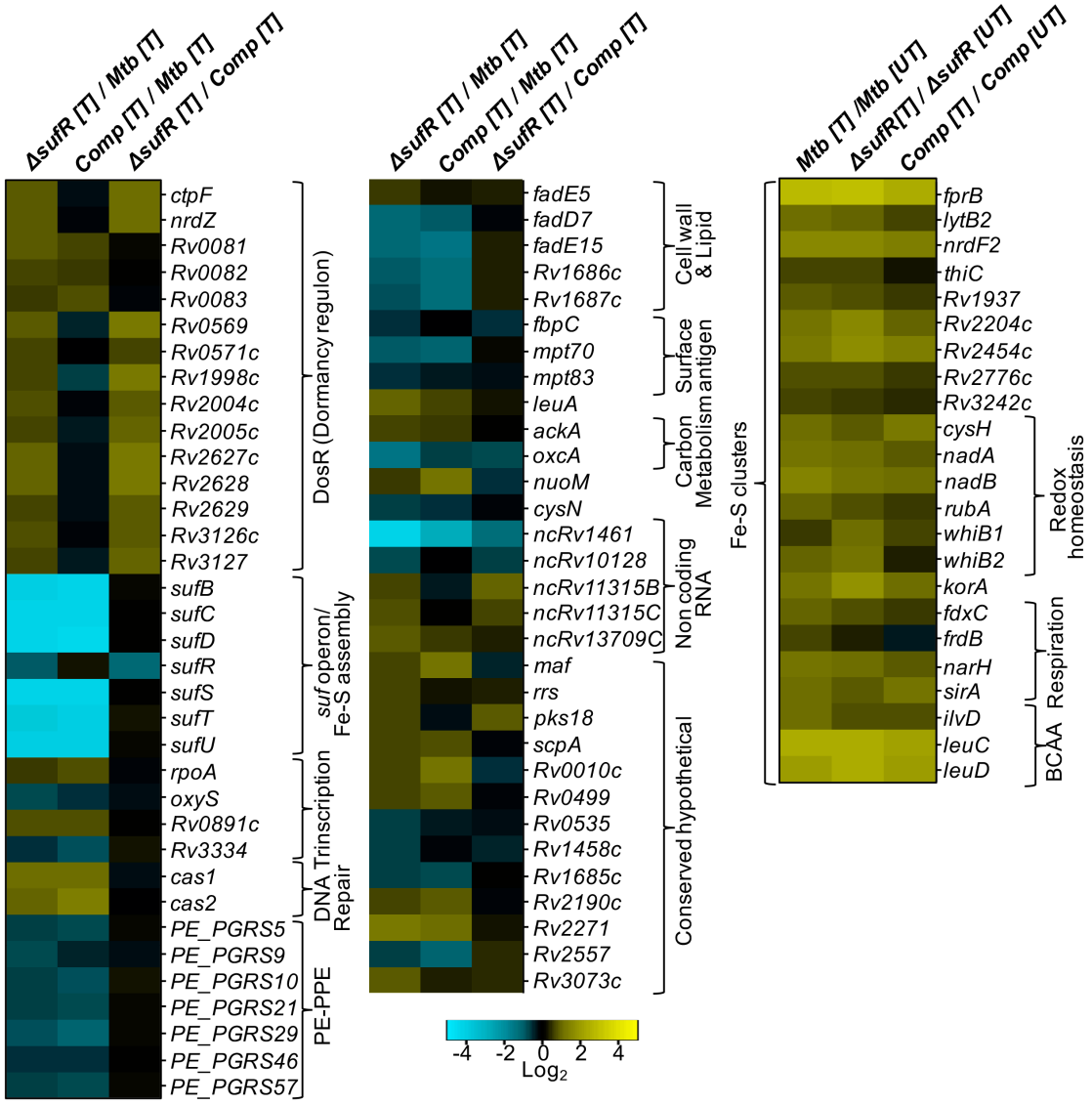

1054

1055 **Figure 3: Transcriptome of *MtbΔsufR* in response to NO.** Total RNA was
1056 isolated from three biological replicates of untreated (UT) and DETA-NO
1057 treated (T) *MtbΔsufR* and *sufR-Comp* and subjected to RNA-seq analysis.
1058 Heat maps indicate log2 fold changes of differentially expressed genes
1059 (DEGs) belonging to various functional categories (obtained from
1060 Mycobrowser, EPFL, Lausanne). Genes were considered differentially
1061 expressed on the basis of the false discovery rate (FDR) of ≤0.05 and
1062 absolute fold change of ≥1.5. "T" and "UT" indicate DETA-NO treated and
1063 untreated conditions, respectively. BCCA: branched chain amino acid.

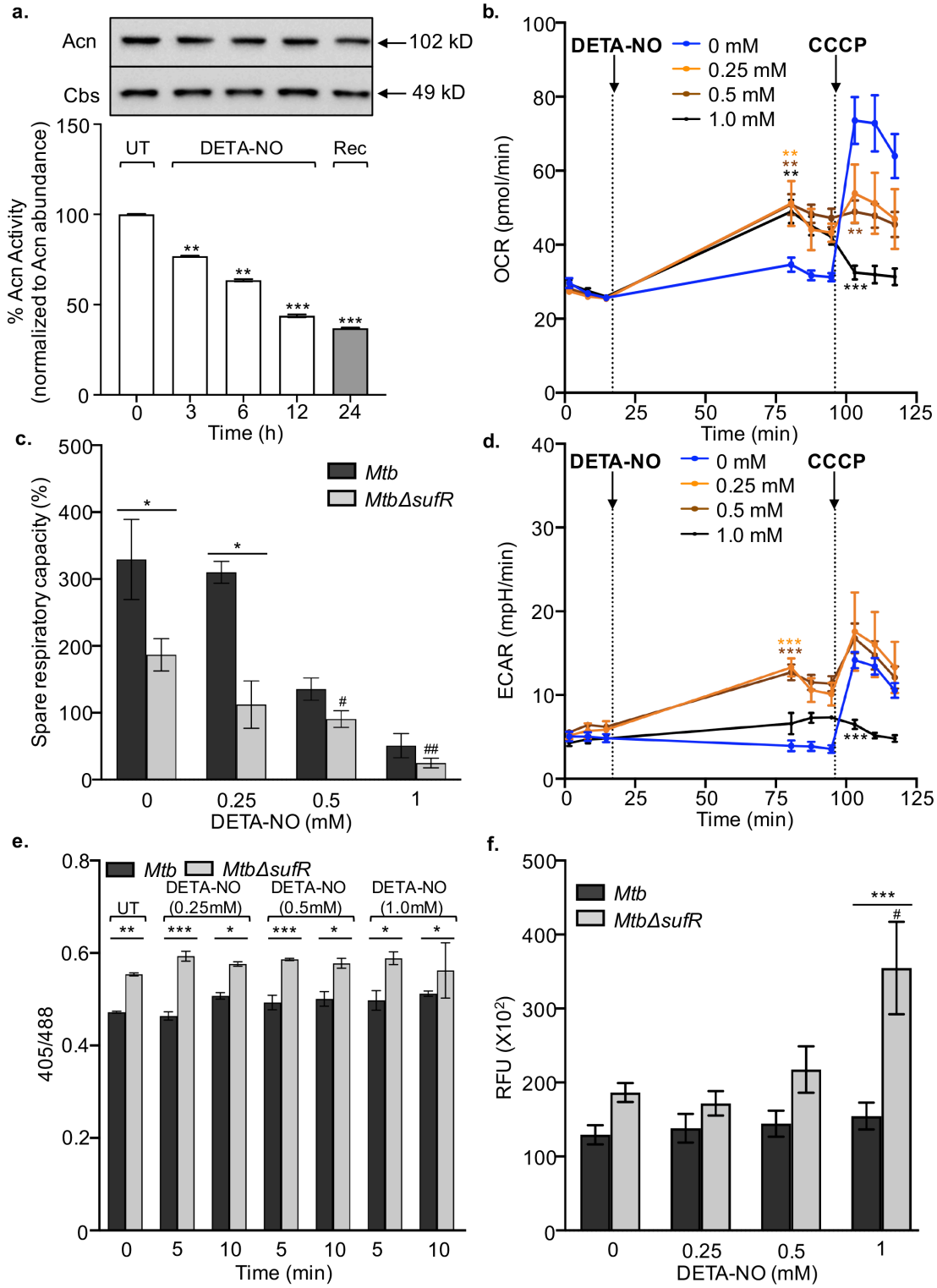

1064

1065 **Figure 4: SufR is required to maintain Fe-S cluster homeostasis,**
1066 **respiratory reserves, and redox balance in response to NO. a)** Acn
1067 activity of *MtbΔsufR* in response to DETA-NO over time. At 12 h post-
1068 treatment, *MtbΔsufR* was cultured in a DETA-NO free 7H9 broth for 24h and

1069 recovery (Rec) of Acn activity was quantified as a measure of Fe-S cluster
1070 repair. Under these conditions, intracellular levels of Acn remained unaltered.
1071 A non Fe-S cluster protein cystathione-β-synthase (Cbs) was used as an
1072 internal loading control. **b)** A change in OCR of *MtbΔsufR* was quantified upon
1073 addition of indicated concentrations of DETA-NO by Seahorse XF flux
1074 analyser. The uncoupler CCCP was used to maximally induce respiration and
1075 to determine the influence of NO on the spare respiratory capacity (SRC). The
1076 first and second vertical lines indicate point of addition of DETA-NO and
1077 CCCP, respectively. **c)** Decrease in SRC of wt *Mtb* and *MtbΔsufR* with
1078 increasing concentrations of DETA-NO. **d)** ECAR of DETA-NO-treated
1079 *MtbΔsufR.* **e**) *Wt Mtb* and *MtbΔsufR* expressing Mrx1-roGFP2 were exposed
1080 to the indicated concentrations of DETA-NO and changes in the biosensor
1081 ratio (405/488 nm) were measured using flowcytometry. **f)** Wt *Mtb* and
1082 *MtbΔsufR* treated with the indicated concentrations of DETA-NO for 2 h was
1083 stained with CellRox Deep Red reagent to measure endogenous ROS. Data
1084 shown are the result of three independent experiments performed in triplicate
1085 (mean ± S.D.). One/two-way analysis of variance (ANOVA) as applicable with
1086 Bonferroni's post hoc test was employed to determine statistical significance
1087 between different doses of DETA-NO. *p* value is <0.05 were indicated with
1088 symbols. Symbols: (*): comparison to untreated *Mtb* control, (#): comparision
1089 to untreated *MtbΔsufR*. Statistical significance for the OCR and ECAR was
1090 obtained by comparing different doses of DETA-NO with untreated,
1091 Comparisons whose P value is <0.05 were indicated with different symbols.
1092 Symbols: (*): comparison to 0.25mM; (*): comparison to 0.5mM; and (*):
1093 comparison to 1.0 mM */*/*/# p<0.05; **/**/**/## p<0.01; ***/***/*** p<0.001.

1094

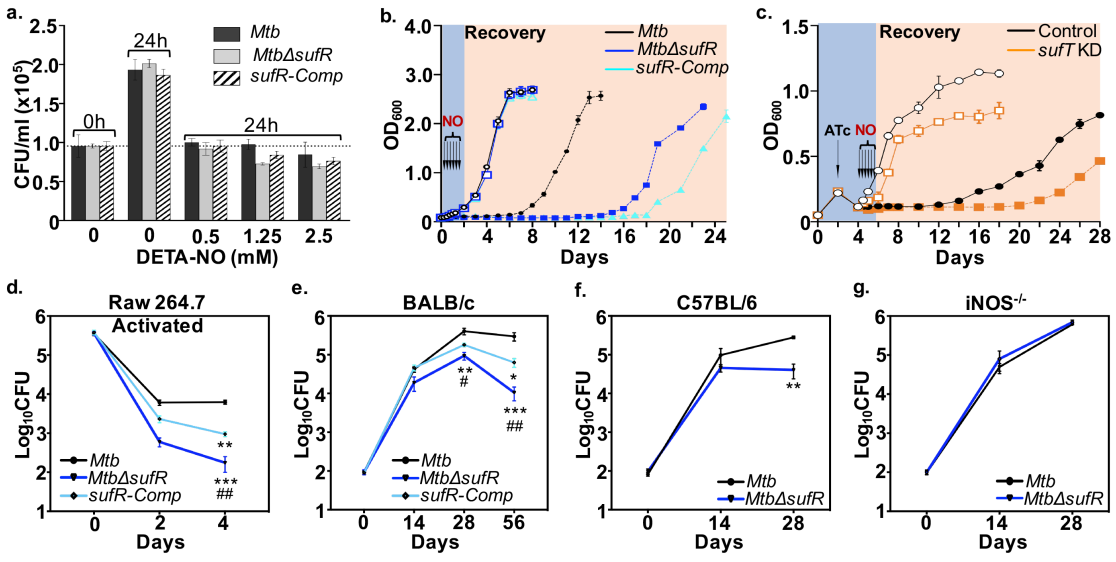

1095

1096 **Figure 5: SufR is required for recovery from NO-induced growth arrest *in***
1097 ***vitro* and NO-dependent persistence *in vivo*. a)** Wt *Mtb*, *MtbΔsufR* and
1098 *sufR-Comp* were exposed to indicated doses of DETA-NO for 24h and
1099 survival was monitored by enumerating CFUs. b) Wt *Mtb*, *MtbΔsufR,* and
1100 *sufR-Comp* were either left untreated (UT) or treated (T) with repeated doses
1101 of 0.1 mM of DETA-NO for 36 h at an interval of 6 h and growth was
1102 monitored over time. **c)** *Mtb* strains expressing CRISPRi vectors without
1103 (vector control) or with *sufT*-specific guide RNA (sgRNA) were left untreated
1104 (UT) or treated (T) with 0.1 mM of DETA-NO at an interval of 6 h for 36 h and
1105 growth was monitored over time**. d**) IFNγ-LPS-activated Raw264.7 cells were
1106 infected with wt *Mtb*, *MtbΔsufR* and *sufR -Comp* strains at moi 10 and
1107 intramacrophage survival was monitored by enumerating CFUS at the
1108 indicated time points. Data are the results of two independent experiments
1109 performed in triplicates. **e)** Inbred BALB/c mice (*n* = 6) were given an aerosol
1110 challenge with *wt Mtb*, *MtbΔsufR* and *sufR-Comp* and assessed for survival in

1111 lungs at indicated time points. Results are expressed as mean ± standard
1112 deviation (SD). f) C57BL/6 (n=5), iNOS$^{-/-}$ knockout (n=5) mice were given an
1113 aerosol challenge with *wt Mtb* and *MtbΔsufR* and assessed for survival in
1114 lungs at indicated time points. Statistical significance for the intramacrophage
1115 and pulmonic load was obtained by comparing different strains, Comparisons
1116 whose *P* value is <0.05 were indicated with different symbols. Symbols: (*):
1117 comparison to *wt Mtb*; (#): comparison to *sufR -comp*. */# p<0.05; **/##
1118 p<0.01; ***/### p<0.001.

1119

1120

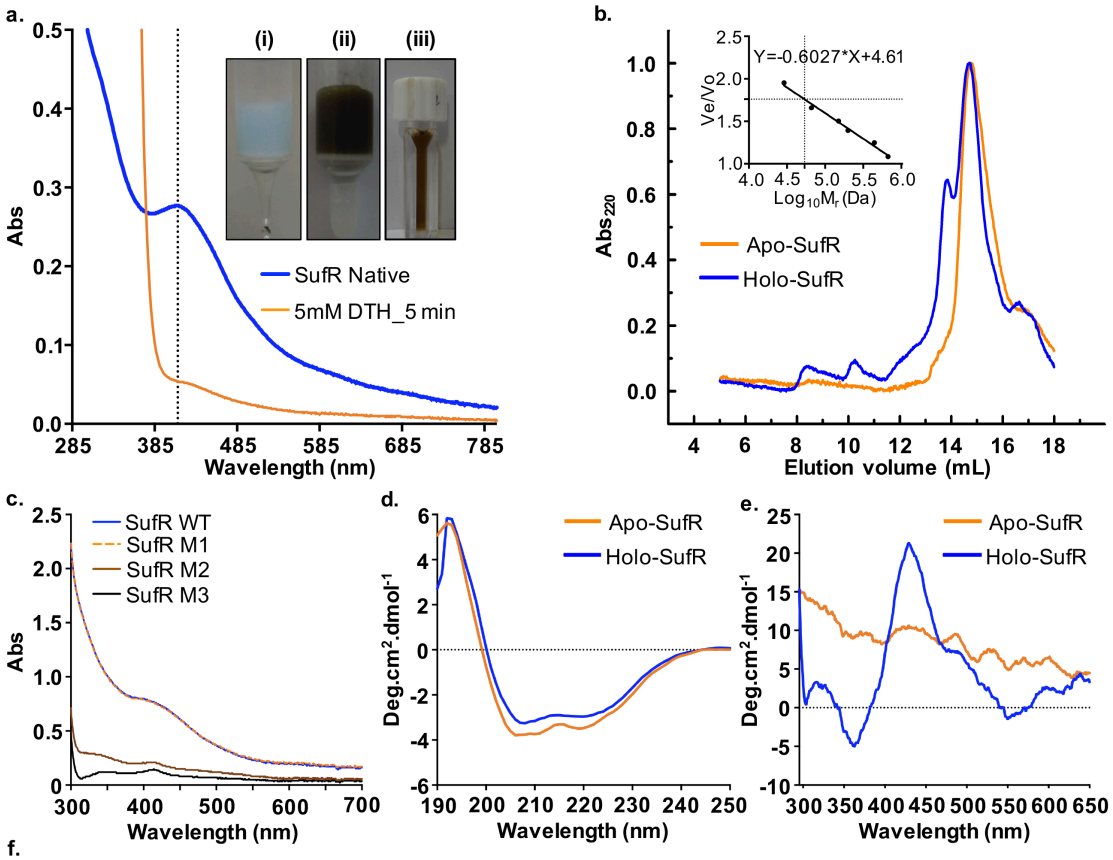

f.

Chemical assay of non-heme iron and acid-labile sulfide of holo-SufR				
	Batch 1	Batch 2	Batch 3	Average
Iron (μM)	300.29±32[b]	295.88±11[c]	259.12±25[d]	291.76±29.27
Sulfide (μM)	287.36±40[b]	286.71±28[b]	277.36±76[d]	285.11±38.46
Protein (μM)	80	80	80	80
Iron/Protein[a]	3.75±0.4	3.7±0.14	3.23±0.32	3.64±0.4
Sulfide/protein[a]	3.59±0.5	3.58±0.35	3.47±0.95	3.54±0.5
Fe:S	1.05±0.08	1.08±0.09	0.95±0.17	1.03±0.1

[a] With reference to the monomer of SufR
[b] Average of four
[c] Average of three
[d] Average of two

1121

1122 **Figure 6: *Mtb* SufR is dimeric and coordinates 4Fe-4S cluster. (a)**
1123 Anaerobically-purified SufR was subjected to UV-visible spectroscopy. A clear
1124 peak at 413 nm indicates presence of a 4Fe-4S cluster. Addition of one
1125 electron reducing agent, dithionite (DTH; 5 mM) caused rapid bleaching of
1126 color and loss of the peak at 413 nm. Inset: **i)** Ni^{2+}-NTA beads free of bound
1127 protein, **ii)** dark brown colored Ni^{2+}-NTA beads due to binding of holo-SufR
1128 under anaerobic condition, and **iii)** anaerobically purified holo-SufR exhibiting
1129 dark brown color. **(b)** Chromatographic profiles of apo- and holo-SufR eluting
1130 from a Superdex 200 HR gel filtration column. (Inset: standard curve

1131 generated from a linear fit of the log molecular weight of the protein standards
1132 versus their elution parameter V_e/V_o where, V_e is the elution volume and V_o is
1133 void volume). Both apo- and holo-SufR eluted at a volume corresponding to a
1134 molecular mass of ~54 kDa. (c) Holo-SufR and cysteine mutants of SufR (M1:
1135 C175A, M2: C175A_C179A; and M3: C175A_C179A_C192A) were purified
1136 anaerobically and scanned by a UV-vis spectrophotometer. The M2 and M3
1137 mutants of SufR showed absence of absorbance at 413 nm indicating loss of
1138 4Fe-4S cluster. (d) A far-UV CD spectrum of holo-SufR from 200 nm to 250
1139 nm wavelength. **(e)** Near-UV CD spectra of apo- and holo- SufR. (**f**) Chemical
1140 estimation of Fe and S content in holo-SufR.
1141
1142

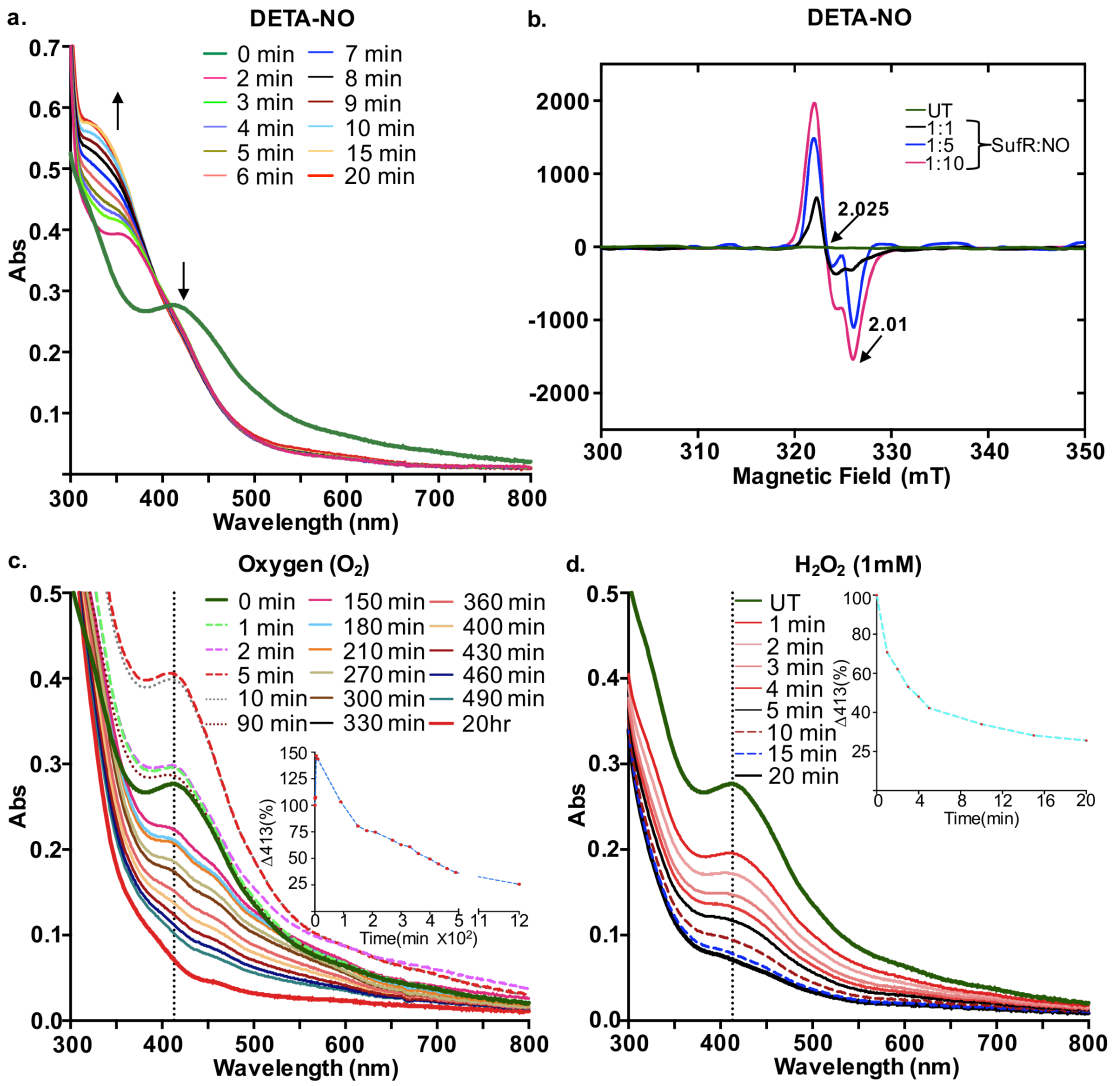

Figure 7: Fig 5: The *Mtb* SufR Fe-S cluster responds to NO and H_2O_2. (a) UV-visible spectra were acquired before and after addition of proline NONOate (2.5 mM). A time dependent increase in the characteristic monomeric DNIC peak at ~ 350 nm was observed in the NO-treated sample. **b**) Holo-SufR was exposed to various concentrations of proline NONOate (1, 5, and 10 -fold molar excess) and EPR spectra were acquired at a microwave frequency of 9.667 GHz and microwave power of 2 mW at liquid nitrogen temperature. The peak at 2.025 *g* is consistent with the formation of monomeric DNIC. **(c)** Holo-sufR was exposed to atmospheric O_2 by bubbling air through the sample for 2 min. UV-visible spectra were acquired before and

1154 after exposure at various time intervals as indicated. **(d)** Holo-SufR was
1155 treated with a fixed concentration of H_2O_2 (1 mM) and absorbance was
1156 monitored over time. The gradual decrease in absorbance around 413 nm
1157 indicates loss of Fe-S cluster. (Inset **c, d**) Rate of the 4Fe-4S cluster loss was
1158 determined by calculating the percent loss of absorbance at 413 nm upon
1159 exposure to air and H_2O_2 at various time intervals.
1160

1161

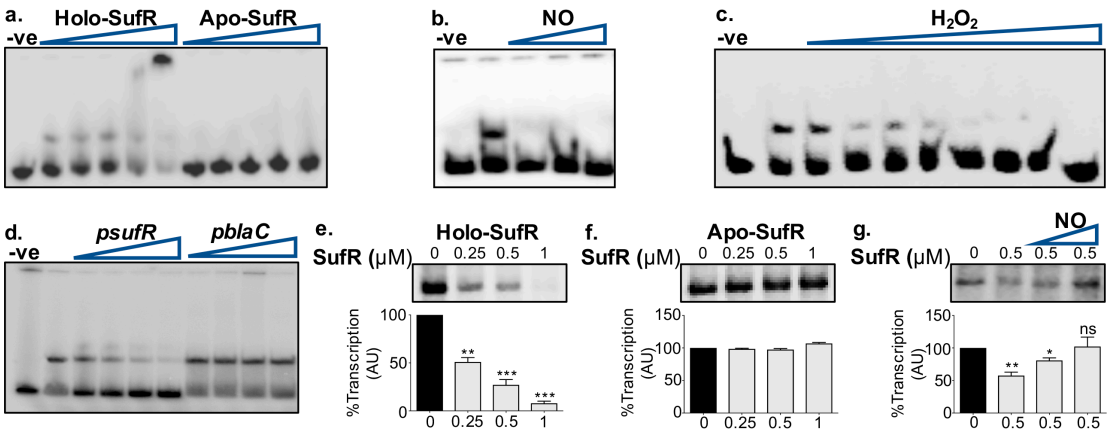

1162

1163 **Figure 8: NO and H_2O_2 trigger loss of SufR binding to the promoter of the**
1164 ***suf* operon. (a)** EMSA of holo- and apo-SufR binding to ^{32}P-labelled *suf*
1165 promoter DNA fragment (0.5 nM). The concentrations of holo- and apo-SufR
1166 used for EMSAs were 0.125 μM, 0.25 μM, 0.5 μM, 1 μM, and 2 μM. Holo
1167 SufR (0.5 μM) was pretreated with **b)** proline NONOate (NO; 2.5-, 5-, and 10-
1168 fold molar excess) or **(c)** H_2O_2 (25, 50, 75, 100, 250, 500, 1000 and 5000 nM)
1169 and were incubated with ^{32}P-labelled *suf* promoter. (**d)** Holo SufR (0.5 μM)
1170 was incubated with ^{32}P-labelled *suf* promoter and DNA binding was competed
1171 out using 12.5-, 25-, 50-, and 100-fold molar excess of unlabelled competitor
1172 promoter fragment of *suf* operon and *blaC.* (e) Effect of holo- and apo-SufR
1173 on transcription from *suf* promoter *in vitro*. Single-round transcription assays
1174 show that RNAP-σA efficiently directs transcription from the *suf* promoter
1175 giving an expected product of 107 bp. Increasing concentrations of holo-SufR
1176 inhibit transcription. **f)** Apo-SufR was completely ineffective in inhibiting
1177 transcription. **g)** Holo SufR (0.25 μM) pre-treated with proline NONOate (NO;
1178 2.5-, and 5 -fold molar excess) stimulated transcription in a dose dependent
1179 manner. The graph below indicates densitometry analysis of the *suf* transcript
1180 (*n*=2). One-way analysis of variance (ANOVA) with Bonferroni's post hoc test

1181 was employed to determine statistical significance. Statistical significance was
1182 obtained by comparing with SufR untreated. '*' $p<0.05$ '**' $p<0.01$ '***'
1183 $p<0.001$.
1184

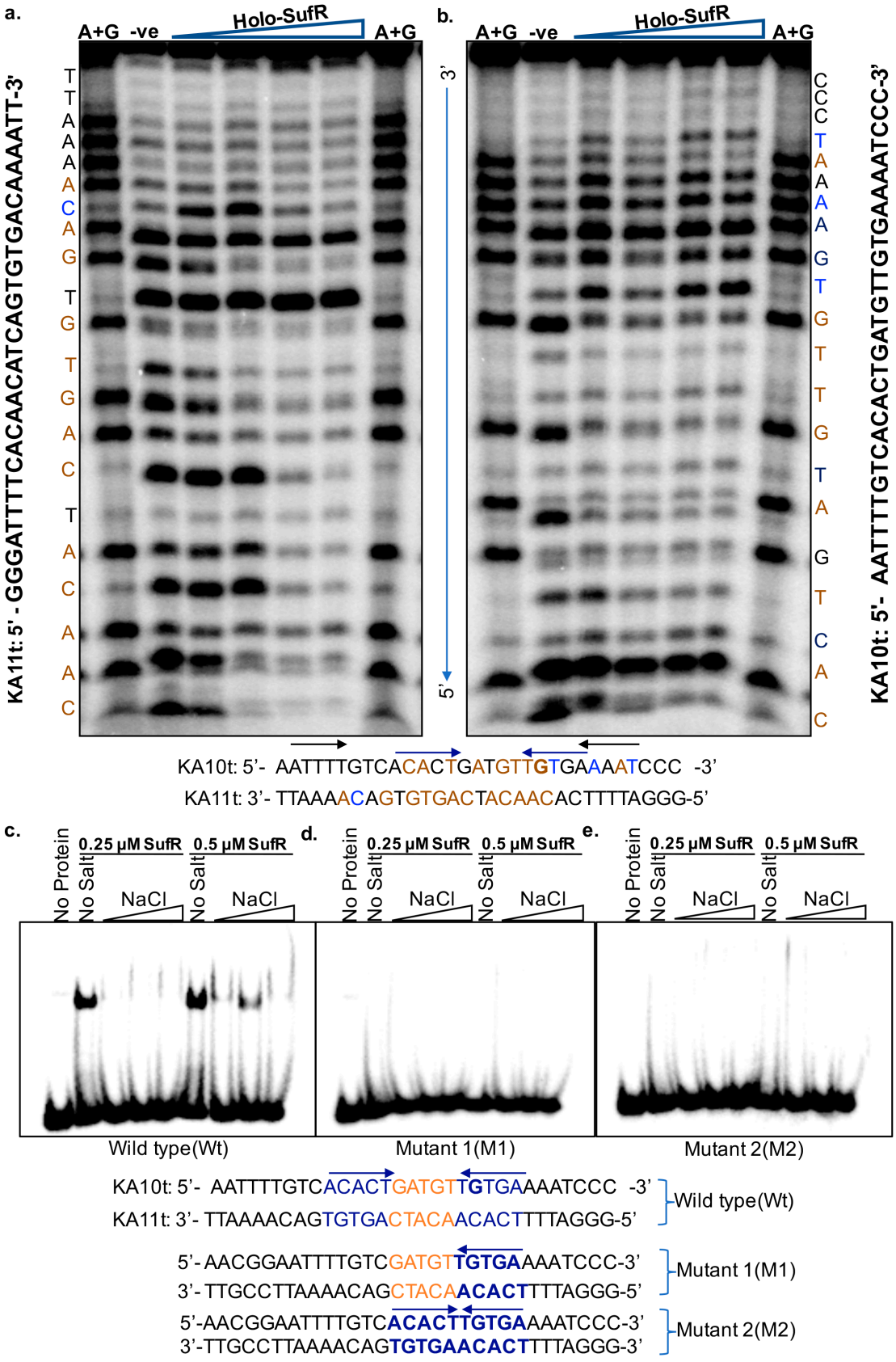

Figure 9: DNase I footprint of holo-SufR bound to *suf* promoter: Sequence upstream of the *suf* operon (KA10t and its complementary strand-

1188 KA11t) were used for DNase I footprint. Bold letter **G** in the sequence is the
1189 transcription start site (TSS) as well start codon for *Mtb* SufR**. (a)** KA10t was
1190 labeled with ^{32}P and annealed with cold KA11t. **(b)** KA11t was labeled with
1191 ^{32}P and annealed with cold KA10 in order to examine the protected region in
1192 the reverse strand. Reactions containing 5 nM ^{32}P-labeled dsDNA substrate
1193 were incubated either in absence or in the presence of increasing
1194 concentration of purified holo-SufR protein (125 nM, 250 nM, 500 nM, 1 μM,).
1195 0.05U of DNase I was added to the reaction mixture and digestion was carried
1196 out for 2 mins at room temperature. A+G is Maxam and Gilbert sequencing
1197 ladder. DNase I protected nucleotides are marked with red and two inverted
1198 repeats are marked by arrow (blue and black). (**c-e**) EMSA was performed
1199 with wild type (KA10t and KA11t) and oligonucleotides with mutations in the
1200 inverted repeats (KA10tm1, KA11tm1, KA10tm2 and KA11tm2) at increasing
1201 concentrations of NaCl at two different concentrations of SufR (0.25 μM and
1202 0.5 μM).
1203

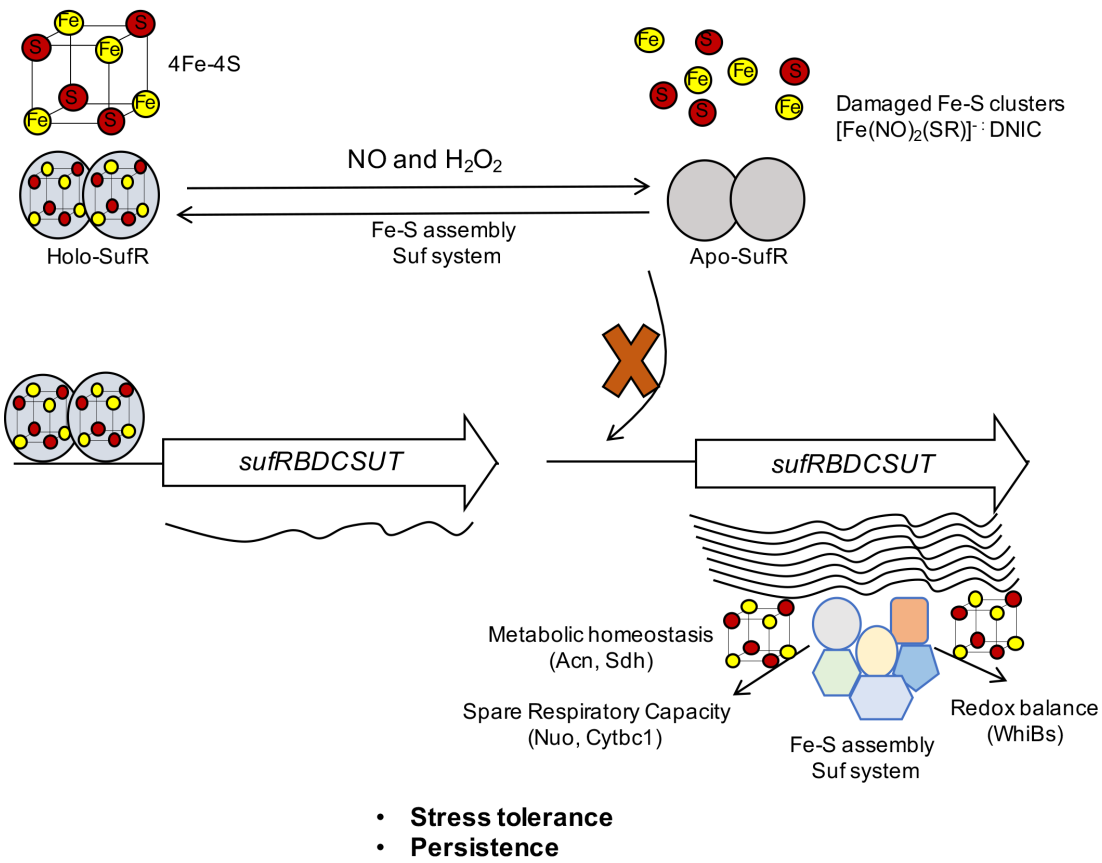

Fig. 10. SufR regulates Fe-S cluster homeostasis in *Mtb*. SufR appears to coordinate the expression of the *suf* operon in a negative feedback loop. Under Fe sufficient conditions, the Fe-S cluster bound form of SufR (holo-SufR) binds to the promoter of the *suf* operon and represses Fe-S biogenesis. Exposure to NO or H_2O_2 damages Fe-S clusters to generate DNIC or apo-forms of SufR, respectively, which abrogates SufR DNA binding resulting in de-repression of the *suf* operon. The elevated expression of the SUF Fe-S assembly system regenerates Fe-S clusters of metabolic enzymes, respiratory complexes, and redox sensors to maintain Fe-S homeostasis, spare respiratory capacity, and redox balance. The NO sensing properties of SufR via its 4Fe-4S cluster and persistence defect exhibited by *MtbΔsufR* in mice in an iNOS-dependent manner suggest that SufR integrates host environmental signals to Fe-S cluster homeostasis in *Mtb*.